Analysis of Strong-Motion Accelerograms

By Shiro TAKADA and Akio KOMATSU

(Manuscript received October 3, 1974)

Abstract

In order to estimate the strain amplitudes occurring in underground structures subjected to earthquakes, data integrating techniques for strong-motion earthquake accelerograph records are investigated.

Excellent base-line corrections and high-pass filtering methods to be attached to integrated velocity and displacement curves are discussed. From the results of numerical integration of 19 accelerograms, empirical formulae related to the maximum velocity amplitude and acceleration, etc. are proposed.

1. Introduction

Relative-displacement distributions in the ground along the structural axis are the most significant factors in the earthquake-resistant design of underground structures, such as gas pipes, water pipes and subway tunnels[1,2].

One of the authors[3] revealed that the axial strains induced in the underground tubular structure during earthquakes are almost proportional to a velocity amplitude of the surrounding ground and that bending strains are proportional to an acceleration amplitude.

Maximum strains are expressed by the following equations;

$$\varepsilon_A=\alpha_A\cdot\frac{V}{v_A},\qquad \varepsilon_B=\alpha_B\cdot\frac{a\cdot A}{(v_B)^2} \tag{1}$$

In this Eq. (1), ε_A and ε_B are the axial and bending strains; v_A and v_B are longitudinal and transversal wave velocities. α_A and α_B are the loss factors which reduce strain levels in the structure by 10–20 percent of those induced in the surrounding ground as the result of interaction between the structure and ground. V and A are the maximum velocity and acceleration of the ground respectively and is a radius of the structure.

Once the maximum acceleration and velocity amplitudes are determined, a rough estimation of the upper bound of the strain induced in the underground tubular structure can be readily calculated from Eq. (1).

Knowledge of maximum-acceleration and velocity levels of the ground during destructive earthquakes is provided by strong-motion accelerograms. It is well known that the ground velocity and displacement curves obtained from the ground acceleration by single or double integration may be subjected to considerable errors over a long period because of the limits of accuracy of base line correction.

The errors present in the raw digitized accelerograms can be divided into two main groups. These are; (1) high-frequency errors due to the fall off of transducer response in the accelerograph, and (2) low-frequency errors caused by mechanism of transducer and digitizing processes, influencing the base-line correction of accelerograms.

For high-frequency errors, digitized data is corrected using by low-pass filter method, and for low-frequency errors, base-line or high-pass filter methods are operated in the processing of uncorrected accelerograms.

In the present paper, to estimate the strain levels in the underground structures, 19 strong-motion accelerograms are singly or doubly integrated using base-line and high-pass filter correction for velocity or displacement curves to preserve a meaningful form. Low-frequency errors present in uncorrected digitized data have little influence over the estimation of strain levels.

Plots of the maximum velocity amplitude or displacement amplitude obtained by numerical integration of accelerograms against the corresponding maximum acceleration amplitude are shown. And resultant empirical formulae enable us to estimate the maximum velocity amplitude when the maximum acceleration for design purpose is given.

2. Base-Line Correction by Polynominal Expressions

Seismograms are recorded on photographic paper on which the zero acceleration level is not indicated. While a zero line must be drawn for digitization purpose, the resulting data would yield unrealistic calculated velocities and displacements without base-line corrections.

Considerable efforts have been made in the past to understand the details of the base-line correction problem. Berg[4], Amin[5] and Shiff[6] assumed the center line as follows;

$$\sum_{i=1}^{3} C_i t^{(i-1)} \tag{2}$$

where the coefficient C_i was determined by the rule that minimize the computed mean-square ground velocity. Minimizing the mean-square ground velocity with respect to the C_i requires;

$$\frac{\partial}{\partial C_i}\int_0^T \dot{x}^2(t)\,dt = 0 \tag{3}$$

where T is the duration of the earthquake record and $\dot{x}(t)$ is the ground velocity.

From the following simultaneous equations, the coefficient C_i may be determined[6];

$$\sum_{j=1}^{3} C_j \frac{T^{(j-1)}}{j(i+j+1)} = B_i - \frac{v_0}{(i+1)T}, \quad i=1, 2, 3 \tag{4}$$

where

$$B_i = \frac{1}{T^{(i+2)}}\int_0^T t^i \cdot \dot{x}_0(t)\,dt, \quad i=1, 2, 3 \tag{5}$$

$$v_0 = \dot{x}_0(0) - \dot{x}(0) \tag{6}$$

and $x_0(t)$ is the uncorrected velocity.

In the present paper, following the precedented method, a five-ordinal base line is assumed. While the higher-ordinal base line give the probability of loss of characteristics contained in uncorrected digitized data, the five-ordinal base line correction would be permissible referring to the literature[7].

Resultant velocities and displacements computed by the five-ordinal base line are compared to that by the three-ordinal base line in the later section.

Coefficients C_i $(i=1\sim5)$ are determined by Eq. (4) as follows;

$$\begin{aligned}
C_1 &= 3675B_1-29400B_2+79380B_3-88200B_4+34650B_5\\
C_2 &= (-58800B_1+501760B_2-1411200B_3+1612800B_4-646800B_5)/T\\
C_3 &= (238140B_1-2116800B_2+6123600B_3+714420B_4+2910600B_5)/T^2\\
C_4 &= (-352800B_1+3225600B_2-9525600B_3+11289600B_4-4656960B_5)/T^3\\
C_5 &= (173250B_1-1617000B_2+4851000B_3-5821200B_4+2425500B_5)/T^4
\end{aligned} \tag{7}$$

3. Integration and High-Pass Filter by Fourier Series Expansion

Generally, time curve $x(t)$ of ground motion during earthquakes can be expressed in the form of the following finite fourier series;

$$x(t)=\frac{A_0}{2}+\sum_{n=1}^{N-1}(A_n\cos\omega_n t+B_n\sin\omega_n t)+\frac{A_N}{2}\cos\omega_N t \tag{8}$$

where

$$A_n=\frac{2}{T}\int_0^T x(t)\cos\omega_n t\cdot dt,\quad B_n=\frac{2}{T}\int_0^T x(t)\sin\omega_n t\cdot dt \tag{9}$$

$$\omega_n=\frac{2n\pi}{T}$$

$2N$ are the number of points plotted on the time curve $x(t)$ at intervals of time step Δt and T is the duration of $x(t)$. Continuous time variable t being transformed into discrete variable $k\cdot\Delta t$, Eq. (8), (9) are rewritten as follows;

$$x_n=\frac{A_0}{2}+\sum_{n=1}^{N-1}\left(A_n\cdot\cos\frac{nk\pi}{N}+B_n\cdot\sin\frac{nk\pi}{N}\right)+\frac{A_N}{2}\cos k\pi \tag{10}$$

$$A_n=\frac{1}{N}\sum_{k=0}^{2N-1}x_k\cdot\cos\frac{nk\pi}{N},\quad B_n=\frac{1}{N}\sum_{k=0}^{2N-1}x_k\cdot\sin\frac{nk\pi}{N} \tag{11}$$

Moreover x_k is expressed as a complex number by the Euler formula;

$$x_k=\frac{\alpha_0}{2}+\sum_{n=1}^{N-1}\frac{\alpha_n}{2}e^{i(nk\pi/N)}+\frac{\alpha_N}{2}e^{i(Nk\pi/N)}+\sum_{n=1}^{N-1}\frac{\alpha_{-n}}{2}e^{-i(nk\pi/N)} \tag{12}$$

where

$$\alpha_n=A_n-iB_n,\quad \alpha_{-n}=A_n+iB_n \tag{13}$$

The next relationship is easily proved to be a fourier coefficient;

$$\alpha_{-n}=\alpha_{2N-n}\quad (n=1, 2, \cdots\cdots, N-1) \tag{14}$$

The fourth item in right hand side in Eq. (12) is transformed using Eq. (14);

$$\sum_{n=1}^{N-1}\frac{\alpha_{-n}}{2}e^{-i(nk\pi/N)}=\sum_{n=1}^{N-1}\frac{\alpha_{2N-n}}{2}e^{i((2N-n)k\pi/N)}=\sum_{n=N+1}^{2N-1}\frac{\alpha_n}{2}e^{i(nk\pi/N)} \tag{15}$$

From Eq. (12), (15), x_k is shown as the following form;

$$x_k=\frac{1}{2}\sum_{n=0}^{2N-1}\alpha_n\cdot e^{i(nk\pi/N)} \tag{16}$$

Consequently x_k and α_n are the complex finite Fourier series and complex finite Fourier coefficients respectively. And x_k is computed quickly and accurately by F.F.T. developed by Cooly and Turkey[8].

From Eq. (10) the integration of time record $x(t)$ is expressed as follows;

$$X(t)=\frac{A_0}{2}t+\sum_{n=1}^{N-1}\left\{-\frac{B_n}{\omega_n}\cos\omega_n t+\frac{A_n}{\omega_n}\sin\omega_n t\right\}+\frac{A_N}{2\omega_N}\sin\omega_N t+C_1 \tag{17}$$

Assuming the initial condition that $X(t)$ is equal to zero at $t=0$, C_1 is that;

$$C_1=\sum_{n=1}^{N-1}\frac{B_n}{\omega_n} \tag{18}$$

$X(t)$ can be expressed in the same Fourier series pattern as $x(t)$ in the following form;

$$X(t)=\frac{A_0'}{2}+\sum_{n=1}^{N-1}\{A_n'\cos\omega_n t+B_n'\sin\omega_n t\}+\frac{A_N'}{2}\cos\omega_N t \tag{19}$$

where

$$A_n'=\frac{2}{T}\int_0^T X(t)\cdot\cos\omega_n t\cdot dt=-\frac{B_n}{\omega_n}$$

$$B_n'=\frac{2}{T}\int_0^T X(t)\cdot\sin\omega_n t\cdot dt=\frac{A_n}{\omega_n}-\frac{A_0T}{2n\pi}$$

$$A_0'=\frac{2}{T}\int_0^T X(t)dt=\frac{A_0T}{2}+2\sum_{n=1}^{N-1}\frac{B_n}{\omega_n} \tag{20}$$

Now, in the case that $x(t)$ is an acceleration time record of ground motion, a velocity time curve could be obtained by operating the above mentioned procedure for once and a displacement time could be calculated repeating the above method again. On the other hand, as mentioned in the previous section, displacement curves obtained by double integration of the acceleration time record is subjected to considerable error over a long period. To eliminate these errors, a high-pass filtering method is frequently useful.

Filtering technique is very easy when the treated record $x(t)$ is expressed in the form of Eq. (8).

Defining the cut-off frequency f_L which should be greater than all frequencies associated with long-period recording and digitizing errors not to be corrected, the filtered curve $x(t)$ becomes;

$$x(t)=\sum_{n=L}^{N-1}\{A_n\cos 2\pi f_n t+B_n\sin 2\pi f_n t\}+\frac{A_N}{2}\cos 2\pi f_N t \tag{21}$$

where

$$f_n = \frac{n}{T} \tag{22}$$

Lower limit frequency f_L should be decided most carefully. Trifunac[9] showed that errors are relatively small in the double-integrated digitized data up to the period of about 16 sec by a study of the properties of the random digitizing errors introduced by the operator.

On the other hand, strain levels induced in the underground structure would not be so much for the case of long-period seismic waves. Therefore displacement spectra for earthquake-resistant design used to construct the Kinuura submerged tunnel[10] were calculated using seismic records of which longer period components were filtered out than 15 sec. In the present computation, f_L is adopted to be 0.06 Hz considering the above studies.

4. Numerical Computation and Discussion

Influences of base-line correction and high-pass filtering operation upon the integrated time curves are investigated by means of several cases. Strong earthquake accelerogram, S544N, obtained at Hosojima in Kyushu (data by The Port and Harbour Research Institute in Japan) is used for the above purposes modifying the maximum acceleration to be 250 gals.

Case 1; Both the base-line correction and high-pass filter operation are not practiced. Fig. 1 shows the acceleration, velocity and displacement curves for this case, which has no physical meanings in the latter two curves. This computation suggests that a base-line correction of some sort or high pass filter is necessary for the present purposes.

Case 2; Base-line correction of three-ordinal line as specified in Eq. (2) which minimizes the mean-square velocity is used and no filter is operated. As can be judged from Fig. 2, it is also true in Case 2, velocity and displacement curves preserve no meaningful forms.

Case 3; Five-ordinal base-line correction of velocity curve specified in Eq. (7) is employed. A high-pass filter is not used as in Case 2. Fig. 3 shows the three curves of ground motion of Case 3. The velocity curve would be simulative to the curves in the next Case 4, 5. However, the displacement curve fluctuates 5 cm about the center of negative displacement value. Therefore the base-line correction only would not be adequate to obtain the meaningful displacement curve from the integration of the acceleration record.

Case 4; Only a high-pass filter is operated using the formulae specified in Eq. (21). The Lower bound of effective frequency f_L is set by 0.06 Hz to cut off the long-period components of more than 16.7 sec contained in the seismic waves. In Fig. 4 are shown the time curves of ground motion in this case.

Both the velocity and displacement curves do not exhibit drifting character. High-pass filter operational method would be a very effective one to compute the velocity or displacement curves by integrating the accelerograms in the case when long-period components in the seismic waves have no significant influences over the

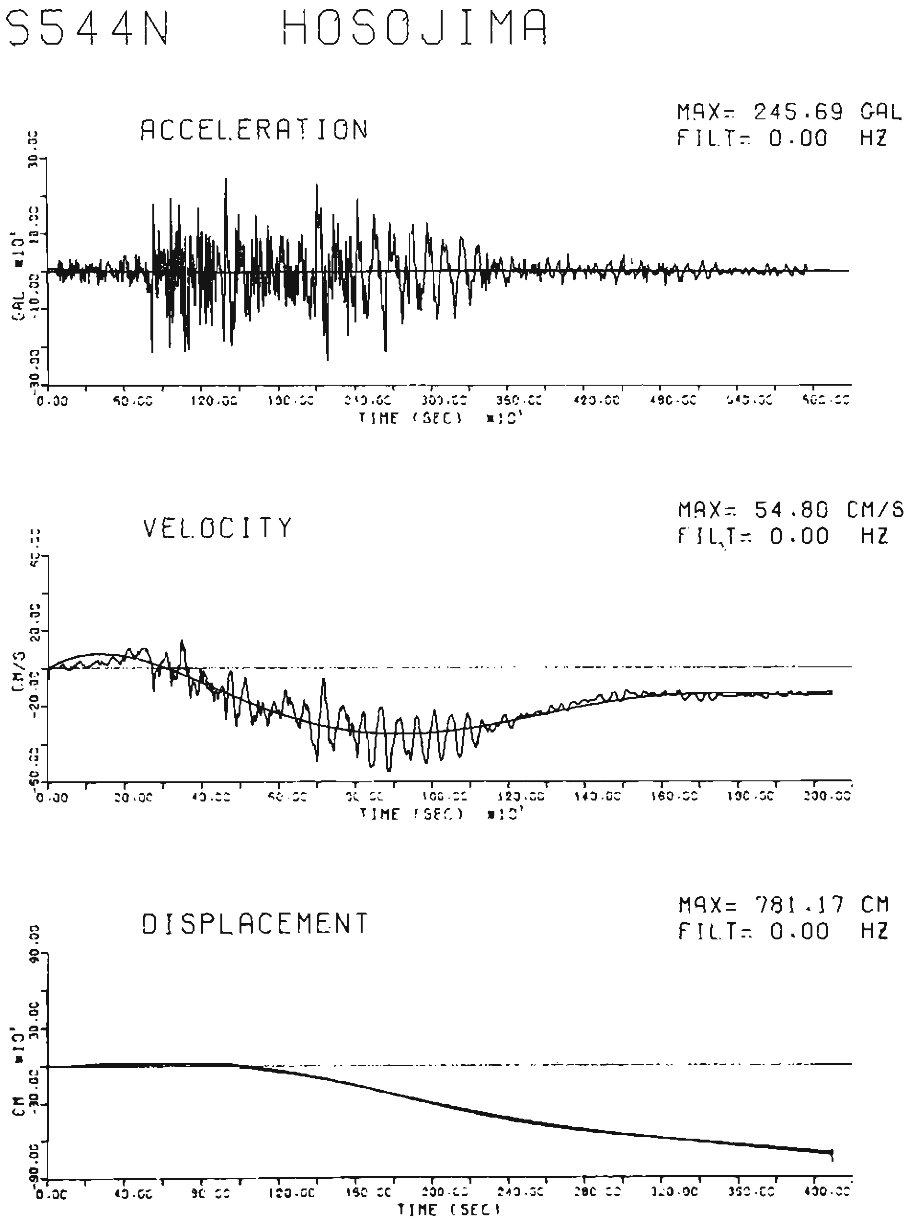

Fig. 1. Uncorrected curves (S544N).

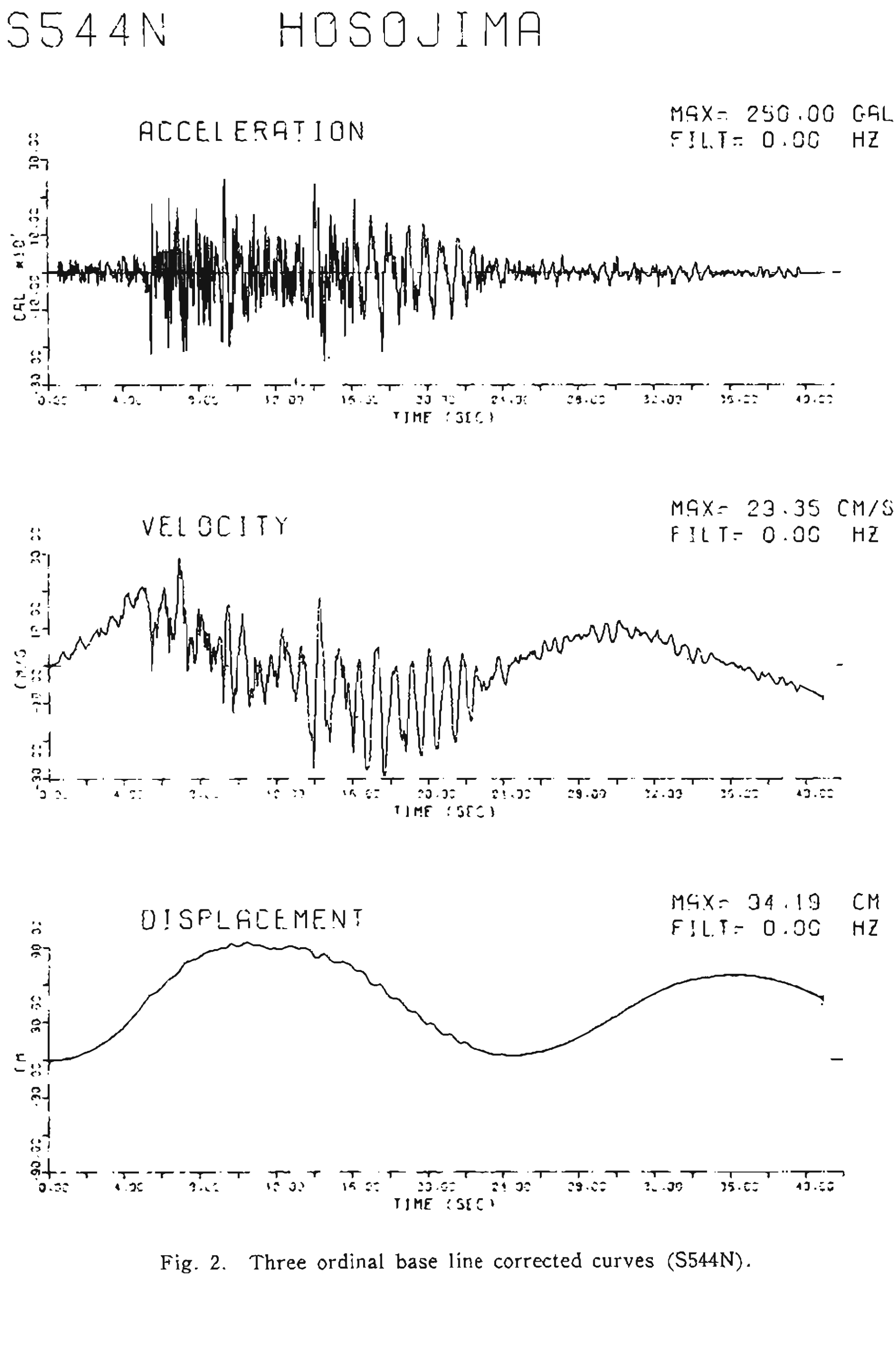

Fig. 2. Three ordinal base line corrected curves (S544N).

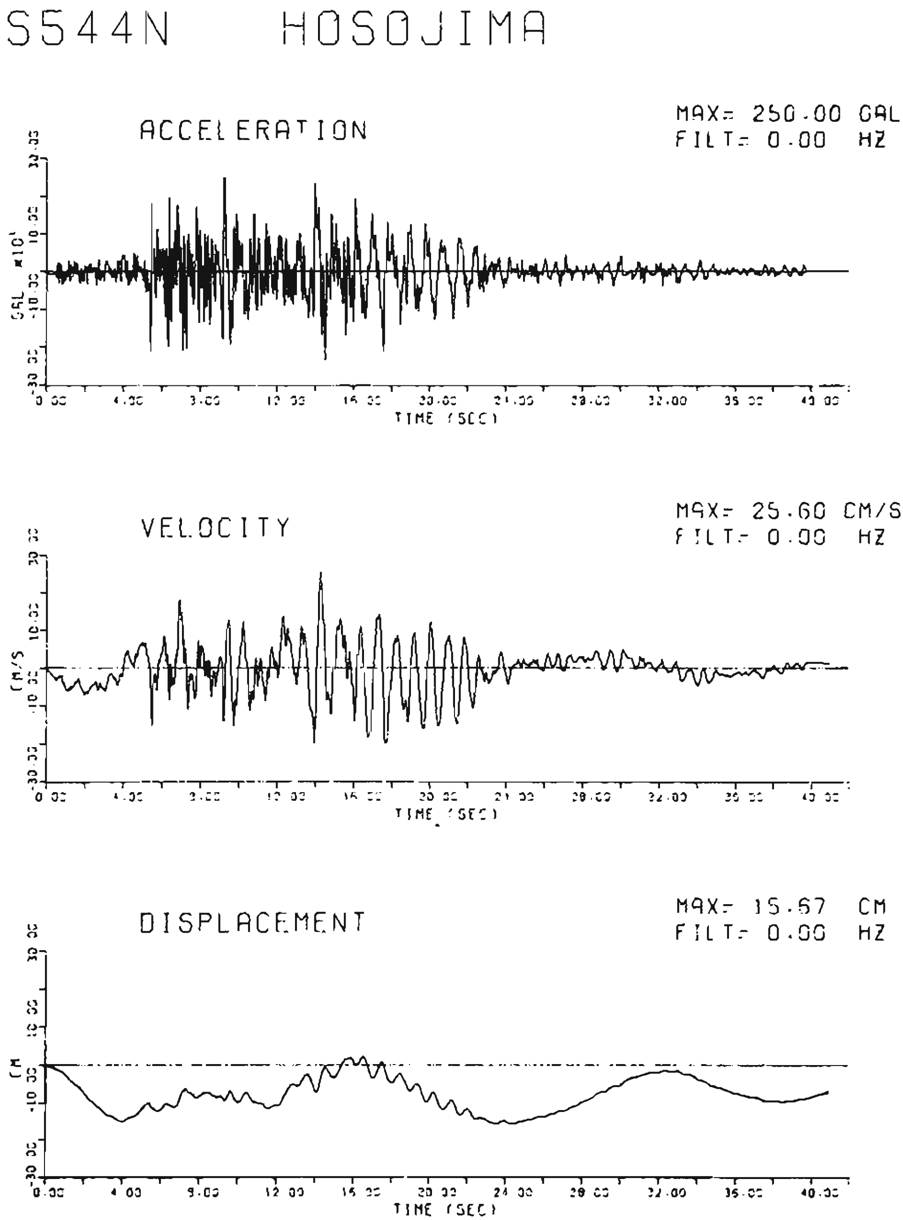

Fig. 3. Five ordinal base line corrected curves (S544N).

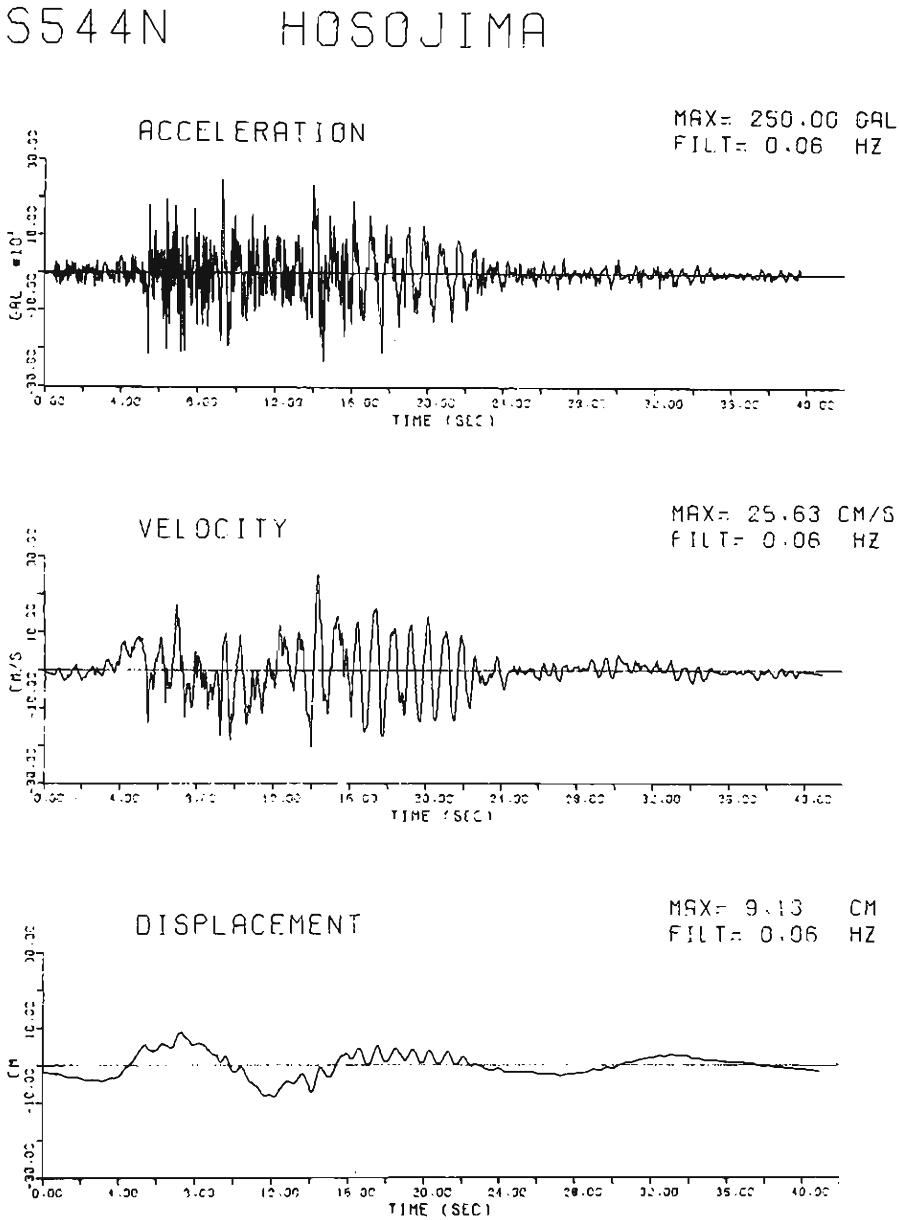

Fig. 4. Filtered curves (S544N).

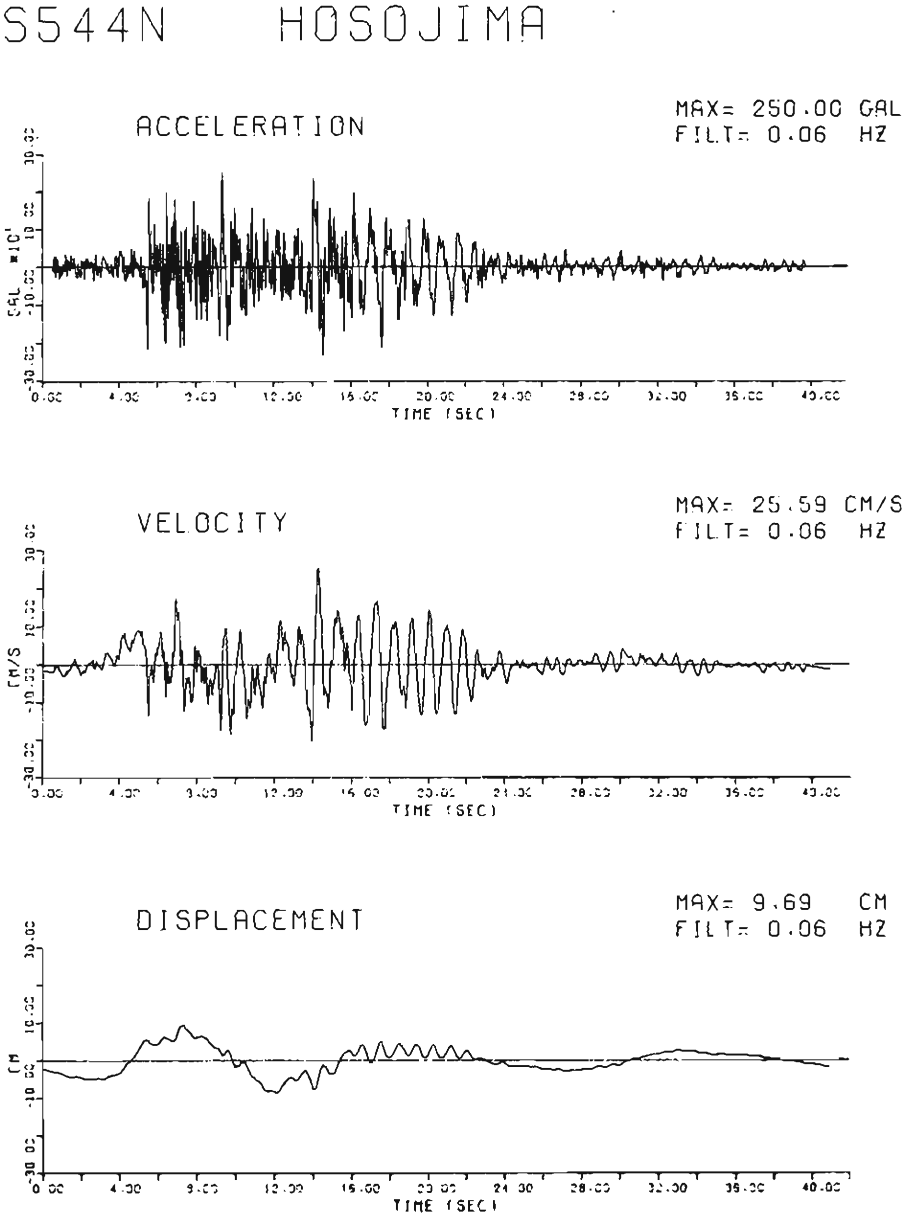

Fig. 5. Base line corrected and filtered curves (S544N).

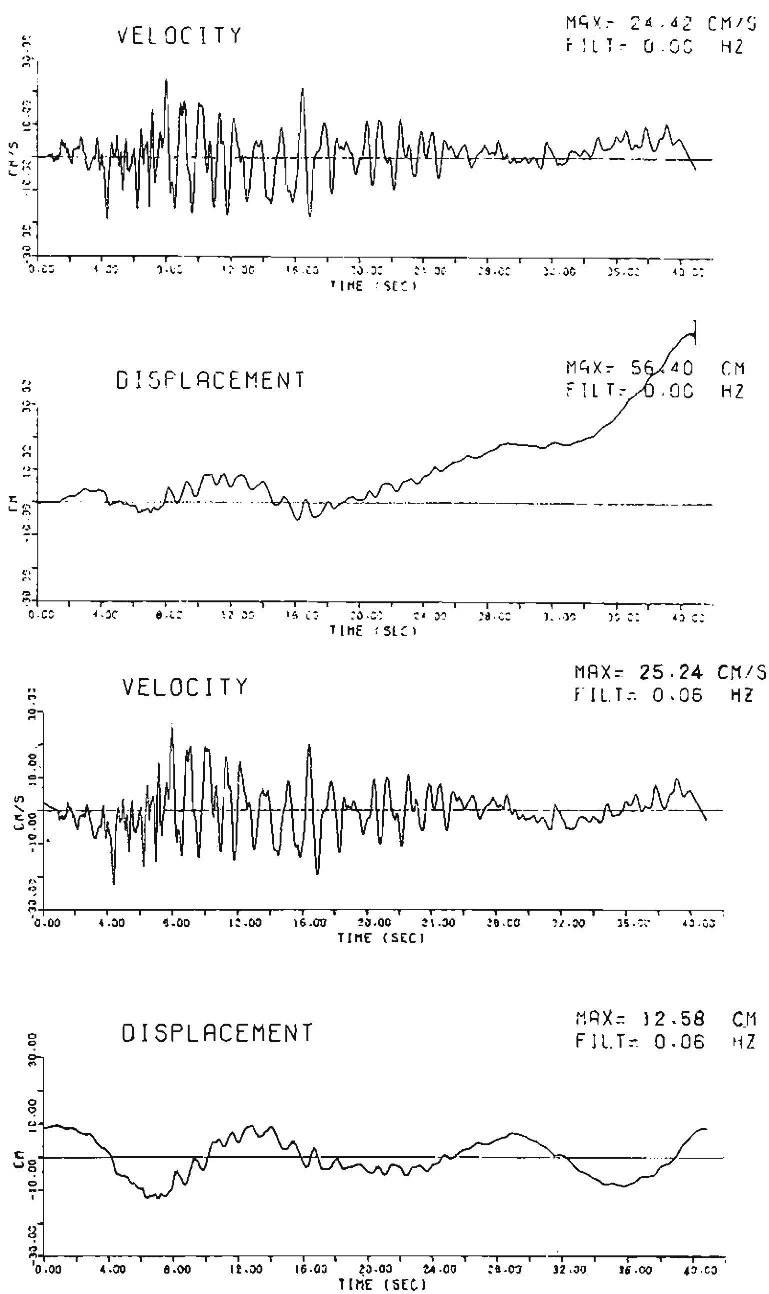

Fig. 6. Comparison between Case 3 and Case 5 (S074).

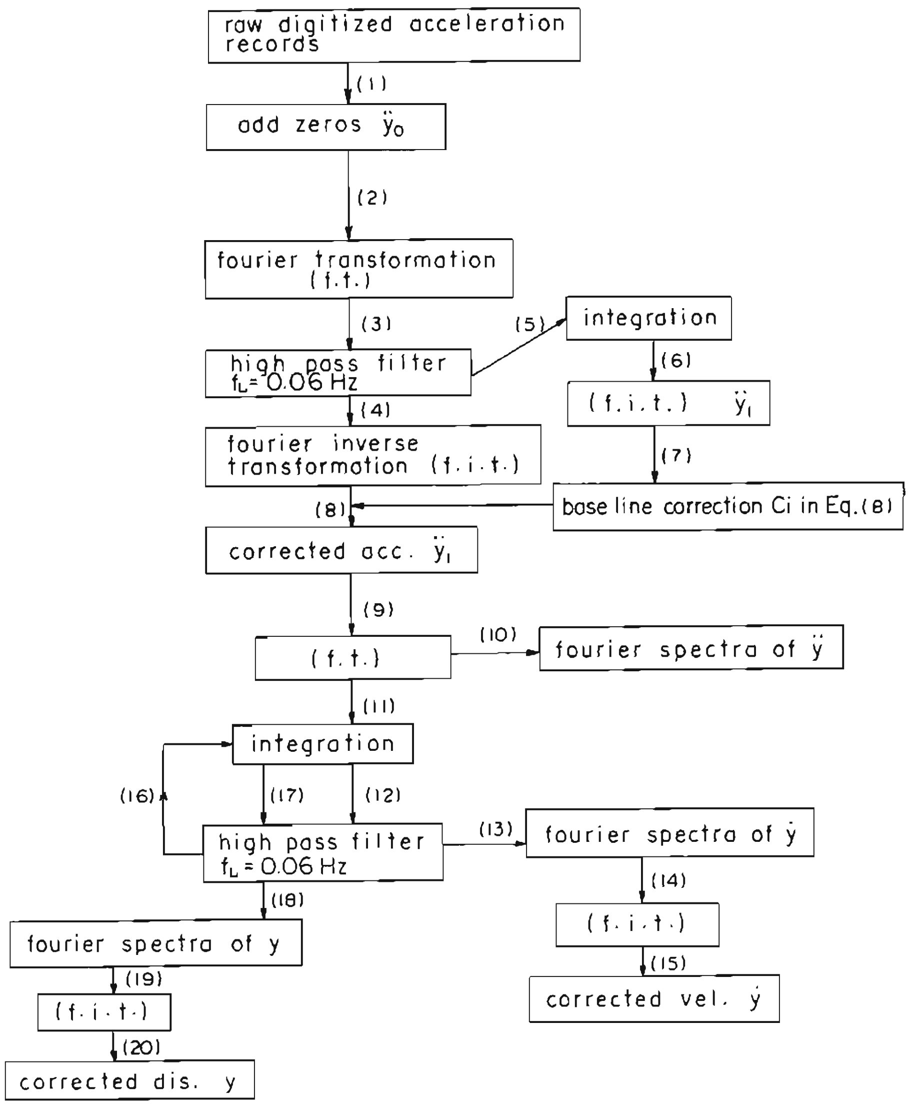

Fig. 7. Flow chart of integration.

results.

Case 5; Both the base-line correction and high-pass filter are used. Integration method used in this case is employed in order to obtain the velocity and displacement curves from after numerical computation. As shown in Fig. 5, velocity and displacement curves are almost the same as that in the Case 4. Differences between Case 4 and Case 5 are 0.16 percent for the maximum velocity and 5.7 percent for the maximum displacement. Moreover, differences between Case 3 and Case 5 are 0.04 percent for the maximum velocity, but 37.7 percent for the maximum displacement. So far as velocity curves are concerned, it would not be difficult to obtain meaningful curves by integrating the acceleration record while judging the above computational results.

However, displacement curves should be calculated taking into consideration the purpose of the curves.

In addition to S544N, earthquake acceleration record S074E recorded at Shimizu in 1965 has been used for the calculation of Case 4 and Case 5. Fig. 6 shows the velocity and displacement curves obtained by integrating S074E by the method specified in Case 4 and Case 5.

The character of velocity curves are similar but the displacement curve being not filtered in Case 4 is drifting and has no physical meaning. In the numerical calculation of present study, the integrating method specified in Case 5 has been employed.

Flow chart of integration procedure is shown in Fig. 7, and the number in the chart indicates the sequence of computation. 19 strong earthquake acceleration records listed in Table 1 are integrated according to the procedures shown in Fig. 7. Among these records, 18 seismograms were recorded by the SMAC B2 seismograph for the past six earthquakes which have occured in Japan during six years from 1965 to 1970. The remaining acceleration record is the one obtained at Taft in 1952.

In Table 1, $N=2^n$ is the total number of data points of digitized accelerations and ND, IO are the number of data points of unmodified acceleration records and additional zeros. Moreover DT is the time interval of data points. All the records are scaled to have the same maximum amplitudes of 250 gals. Several details of the six earthquakes are shown in Table 2.

And computational resultant informations known from velocity, displacement curves and their Fourier spectra are also listed in Table 2.

As the appendixes, acceleration, velocity and displacement curves in time domains and their Fourier spectra in the frequency domains are shown. In these figures, maximum values, filtered lower-limit frequencies and predominant periods are printed.

We could know the various significant characteristics as to ground motions during earthquakes from the resultant time curves and Fourier spectra. It would be useful to reduce the correlative relationships among maximum acceleration, velocity, displacement and predominant period of the ground for the purpose of earthquake resistant design of underground structures.

Table 1. Data of acceleration records used for analyses.

Epicenter	Record No.	N	ND	IO	DT	Station	Date
Near Wakayama	S 265 N	1024	980	10	0.01	Wakayama	1968. 3.30
	S 265 E	〃	〃	〃	〃		
Coast of Iwate Pref.	S 573 N	4096	3930	50	0.01	Miyako	1970. 4. 1
	S 537 E	〃	〃	〃	〃		
Off Miyazaki Pref.	S 544 N	4096	3930	50	0.01	Hosojima	1970. 2.26
	S 544 E	〃	〃	〃	〃		
Tokachi Oki	S 252 N	4096	4000	50	0.01	Hachinohe	1968. 5.16
	S 252 E	〃	〃	〃	〃		
	S 236 N	4096	3940	50	0.01	Miyako	
	S 236 E	〃	〃	〃	〃		
	S 234 N	4096	4000	50	0.01	Muroran	
	S 234 E	〃	〃	〃	〃		
Tokachi Oki	S 241 N	4096	3950	50	0.01	Muroran	1968. 5.16
	S 241 E	〃	〃	〃	〃		
	S 271 N	4096	3960	50	0.01	Miyako	
	S 271 E	〃	〃	〃	〃		
Suruga	S 074 N	4096	3950	50	0.01	Shimizu	1965. 4.20
	S 074 E	〃	〃	〃	〃		
Kern Country	II A 004	2048	1510	25	0.02	Taft	1952. 6.21

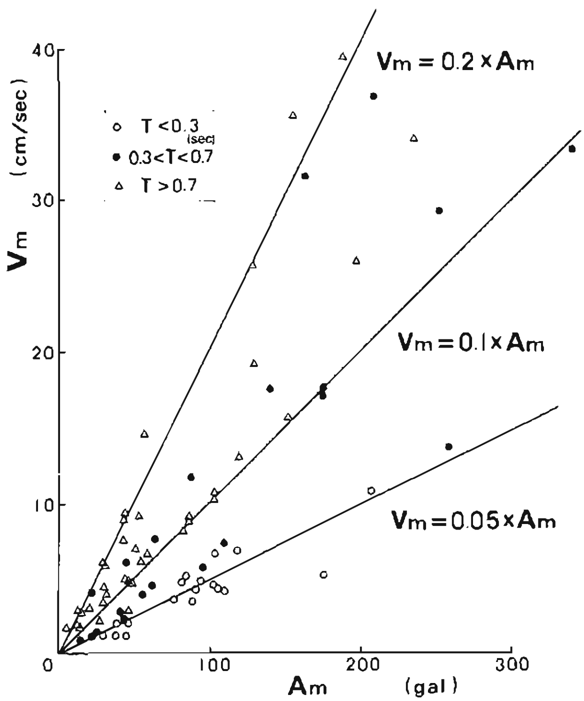

Fig. 8. Relationships between maximum acceleration and maximum velocity.

Table 2. Integrated results of acceleration records by P.H.R.I.

Time and Date	Location of Epicenter	Magnitude	Station	Epicentral Distance (km)	Record No.	Predominant Period (sec)	Max. Acc. (gal)	Max. Vel. (cm/sec)	Max. Dis. (cm)
1968. 3.30 04 : 04	Near Wakayama 34.2°N, 135.1°E		Wakayama 34°13′12″N, 135°09′03″E	5.1	S 265 N S 265 E	0.19 0.51	176 258	5.35 12.90	0.92 1.55
1970. 4. 1 23 : 23	Coast of Iwate Prof. 39.8°N, 142.1°E		Miyako 32°25′57″N, 131°18′38″E	21.7	S 537 N S 537 E	0.17 0.15	111 86	1.16 3.56	1.96 2.37
1970. 2.26 07 : 11	Off Miyazaki Pref. 32.1°N, 132.0°E	6.7	Hosojima 32°25′57″N, 131°18′58″E	10.0	S 544 N S 544 E	0.93 0.77	85 119	8.71 13.01	3.10 7.16
1968. 5.16 09 : 49	Tokachi Oki 40.7°N, 143.7°E	7.8	Hachinohe 40°33′N, 141°29′E	188.3	S 252 N S 252 E	2.73 1.14	235 188	34.01 39.44	11.14 24.91
			Miyako 39°38′N, 141°58′E	189.3	S 236 N S 236 E	0.22 0.19	118 95	6.85 4.99	3.89 3.78
			Muroran 42°19′N, 140°58′E	290.2	S 234 N S 234 E	0.49 0.55	209 140	36.68 17.62	18.86 11.66
1968. 5.16 19 : 39	Tokachi Oki 40.7°N, 143.7°E	7.4	Muroran 42°19′N, 140°58′E	217.9	S 241 N S 241 E	0.42 0.48	95 62	5.84 4.51	2.78 3.33
			Miyako 39°38′N, 141°58′E	226.4	S 271 N S 271 E	0.20 0.19	91 75	4.30 3.71	3.96 3.35
1965. 4.20 08 : 42	Suruga 34.9°N, 138.4°E	6.2	Shimizu 34°59′27″N, 138°30′04″E	13.6	S 074 N S 074 E	1.28 1.24	86.3 102.5	9.04 10.35	4.70 5.16

Table 3. Integrated results of acceleration records by Cal. Tech.

Time and Date	Location of Epicenter	Magnitude	Station	Epicentral Distance (km)	Record No.		Predominant Period (sec)	Max. Acc. (gal)	Max. Vel. (cm/sec)	Max. Dis. (cm)
1940. 3.18 20 : 37	Imperial Valley 32°44′N, 115°27′W	6.3	El Centro 32°47′43″N, 115°32′55″W	11.6	II A001	S00E	0.68	341.7	33.4	10.9
						S90W	0.43	210.1	36.9	19.8
						V	0.12	206.3	10.8	5.6
1951.10. 7 20 : 11	North West Calif. 40°17′N, 124°48′W		Ferndale 40°34′00″N, 124°15′00″W	56.7	II A002	S44W	0.38	102.0	4.8	2.4
						N46W	0.65	109.5	7.4	2.7
						V	0.69	26.4	2.2	1.6
1952. 6.21 04 : 53	Kern Country 35°00′N, 119°02′W	7.7	Pasadena 34°08′20″N, 118°07′17″W	127.2	II A003	S00E	0.68	46.5	6.2	2.7
						S90W	0.97	52.1	9.1	2.9
						V	1.00	29.3	4.5	3.0
			Taft 35°09′00″N, 119°27′00″W	41.5	II A004	N21E	0.74	152.7	15.7	6.7
						S69E	0.34	175.9	17.7	9.2
						V	0.23	102.9	6.7	5.0
			Santa Barbara 34°25′28″N, 119°42′05″W	88.6	II A005	N42E	0.54	87.8	11.8	4.6
						S48E	0.93	128.6	19.3	5.8
						V	0.88	43.6	5.0	2.2
			Hollywood 34°05′00″N, 118°20′00″W	120.8	II A006	S00W	1.03	54.1	6.1	5.1
						N90E	0.92	43.5	9.4	5.9
						V	0.69	22.5	4.2	2.2
			Hollywood 34°05′00″N, 118°20′00″W	120.8	II A007	S00W	1.03	58.1	6.6	4.5
						N90E	0.88	41.2	8.9	6.4
						V	0.73	20.3	3.0	3.4
1954.12.21 11 : 56	Eureka 32°38′N, 117°07′W		Eureka 40°48′00″N, 124°09′00″W	1105.2	II A008	N11W	0.41	164.5	31.6	12.4
						N79E	0.67	252.7	29.4	14.1
						V	1.85	81.3	8.2	4.7
1955. 9. 4 18 : 01	San Jose 37°22′N, 121°47′W		San Jose Bank 37°20′00″N, 121°53′00″W	9.6	II A000	N59E	0.22	105.8	4.4	1.7
						N31W	0.77	100.2	10.8	2.8
						V	0.22	44.2	1.2	1.2
1956. 2. 9 06 : 33	El Alamo Baja Calif. 31°45′N, 115°55′W		Elcentro 32°47′43″N, 115°32′55″W	122.1	II A001	S00W	1.64	32.4	4.0	2.4
						S90W	1.15	50.1	7.0	4.1
						V	1.23	12.4	2.9	1.6

Table 3. Continue

1956. 2. 9 07 : 25	El Alamo Baja Calif. 31°45′N, 115°55′W		Elcentro 32°47′43″N, 115°32′55″W	122.1	II A012	S00W S90W V	1.69 2.08 12.50	11.8 15.4 3.7	1.9 2.7 1.8	1.7 2.3 2.9
1957. 3.22 11 : 44	San Francisco 37°40′N, 122°29′W	5.3	San Francisco 37°48′00″N, 122°24′00″W Soutern Pacific Building	16.6	II A013	N45E N45W V	1.32 1.15 0.52	45.9 44.9 26.8	2.9 5.0 1.5	1.1 1.4 0.9
			San Francisco 37°47′00″N, 122°24′00″W Alexander Bldg Basement	15.0	II A014	N09W N81E V	0.30 0.25 0.23	41.8 45.4 30.0	2.9 2.1 1.3	1.3 1.0 0.4
			San Francisco 37°46′12″N, 122°28′42″W Golden Gate Park	11.6	II A015	N10E S80E V	0.25 0.14 0.11	81.8 102.8 37.2	4.9 4.6 1.2	2.3 0.8 0.7
			San Francisco 37′47′00″N, 122°25′00″W State Bldg Basement	14.3	II A016	S09E S81W V	0.28 0.45 0.34	83.8 55.1 43.5	5.1 4.0 2.3	1.1 0.9 0.6
			Oakland 37°48′00″N, 122°16′00″W	24.3	II A017	N26E S64E V	0.26 0.51 0.52	39.0 23.7 15.3	2.0 1.2 0.9	1.5 1.1 1.3
1961. 4. 8 23 : 23	Hollister 36°40′N, 121°18′W	5.6	Hollister 36°51′00″N, 121°24′00″W	22.3	II A018	S01W N89W V	0.55 0.42 0.74	63.4 175.7 49.1	7.8 17.1 4.7	2.8 3.8 2.2
1968. 4. 8 18 : 30	Borrego 33°09′N, 116°08′W	6.5	Elcentro 32°47′43″N, 115°32′55″W	67.8	II A019	S00W S90W V	1.79 1.61 3.57	127.8 56.3 29.7	25.8 14.7 3.4	12.2 11.0 3.9
			San Diego 32°42′25″N, 117°09′18″W	108.1	II A020	S00W N90E V	3.85 2.13 1.32	29.5 28.9 12.7	6.0 6.1 1.9	4.4 3.0 1.3
1954.12.21 11 : 56	Eureka 32°38′N, 117°07′N		Ferndale 40°34′00″N, 124°15′00″W	1088.7	II A009	N44E N46W V	1.72 1.59 2.00	155.7 197.3 41.9	35.6 26.0 7.6	14.2 9.6 3.9

In addition to the above computational results, integrated results of 60 seismograms by the Earthquake Engineering Research Laboratory of Cal. Tech. are appropriate for the present purposes. Data on these earthquakes and obtained maximum values of acceleration, velocity and displacement are tabulated in Table 3.

First, in Fig. 8 are shown the plots of maximum velocity amplitude obtained by the numerical integration of accelerograms against the corresponding maximum acceleration amplitude. These accelerograms are classified into three groups depending on their predominant period T as shown in the figure. Denoting the maximum acceleration amplitude by A_m and the maximum velocity amplitude by V_m, the following approximate representations are possibly adopted for each group;

$$\begin{aligned} T>0.7\,; &\quad V_m \approx 0.2 \times A_m \\ 0.7>T>0.3\,; &\quad V_m \approx 0.1 \times A_m \qquad (23) \\ T<0.3\,; &\quad V_m \approx 0.05 \times A_m \end{aligned}$$

$(T\,;\ \text{sec},\ V_m\,;\ \text{cm/sec},\ A_m\,;\ \text{gal})$

More important results are obtained concerning the relationship of the maximum velocity amplitude to the predominant period of the corresponding accelerograms, which is shown in Fig. 9. In advance of the computation, all the records are scaled to have the same maximum amplitude of 250 gals.

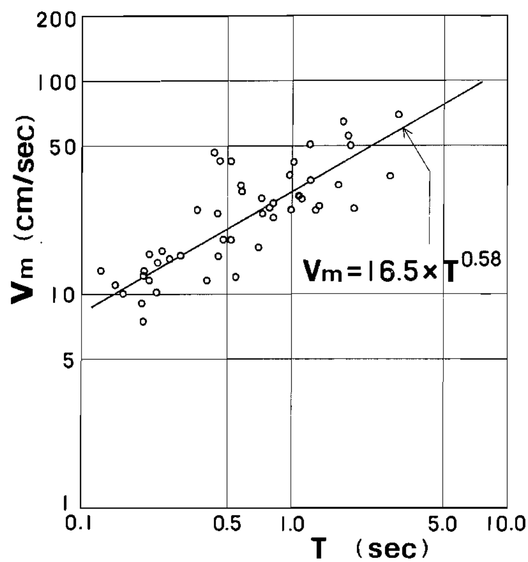

Fig. 9. Relationships between maximum velocity and predominant period.

Applying the least square method to these plots, the following expression is obtained;

$$V_m \approx 16.5 \times T^{0.58} \quad (\text{for } A_m = 250 \text{ gals})$$

These empirical formulae enable us to estimate the maximum velocity amplitude when the maximum acceleration for the design purpose is given.

Once the maximum acceleration and velocity amplitudes are determined, a rough estimate of the upper bound of the strains induced in the underground tubular structures are readily calculated from Eq. (1).

5. Conclusions

The present integrating techniques as shown in Fig. 7 would be able to be used for calculation of ground velocity and displacement curves at a very useful level of engineering significance in order to estimate the strain levels of underground structures. Moreover, Eq. (23), (24) are the significant formulae for the knowledge of the ground motion during earthquakes, and for the earthquake-resistant design purpose of the underground structure.

Acceleration, velocity and displacement curves and Fourier spectra presented in appendix would be very suggestive for the various problems of earthquake engineering.

References

1) Sakurai, A. and Takahashi, T.; Dynamic Stresses of Underground Pipe Lines during Earthquakes, Proc. of the 4th WCEE, 1969, pp. 81-95.
2) Kuessel, T. R.; Earthquake Design Criteria for Subways, Proc., ASCE, ST6, 1969, pp. 1213-1231.
3) Goto, H., Toki, and Takada, S.; Vibrational Characteristics of Underground Pipe, Annuals of Disaster Prevention Research Institute, Kyoto Univ., No. 15B, 1972, pp. 513-526.
4) Berg, G. V. and Housner, G. W.; Integrated Velocity and Displacement of Strong Earthquake Ground Motion, BSSA, Vol. 51, No. 2, 1961.
5) Amin, M. and Ang, A. H.; A Nonstationary Stochastic Model for Strong Motion Earthquakes, Civil Engineering Studies, Structural Research Series, No. 306, University of Illinois, Urbana, 1966.
6) Schiff, A. and Bogdanoff, J. L.; Analysis of Current Methods of Integrating Strong Motion Accelerograms, BSSA, Vol. 57, No. 5, 1967.
7) Kurihara, C. and Sakurai, A.; Integration of Earthquake Acceleration, Central Research Institute of Electric Power Industry Technical Report No. 68077, 1968.
8) Cooley, J. W. and Turkey, T. W.; An Algorithm for Machine Calculation of Complex Fourier Series, Mathematical Compution, Vol. 90, 1964, pp. 297-301.
9) Trifunac, M. D., Udwadia, F. E. and Brady, A. G.; Analysis of Errors in Digitized Strong Motion Accelerograms, BSSA, Vol. 63, No. 1, 1973, pp. 157-187.
10) Aoki, Y.; Seismic Design Criteria for Trench Type Tunnel, JSSA, No. 211, 1973, pp. 77-87.

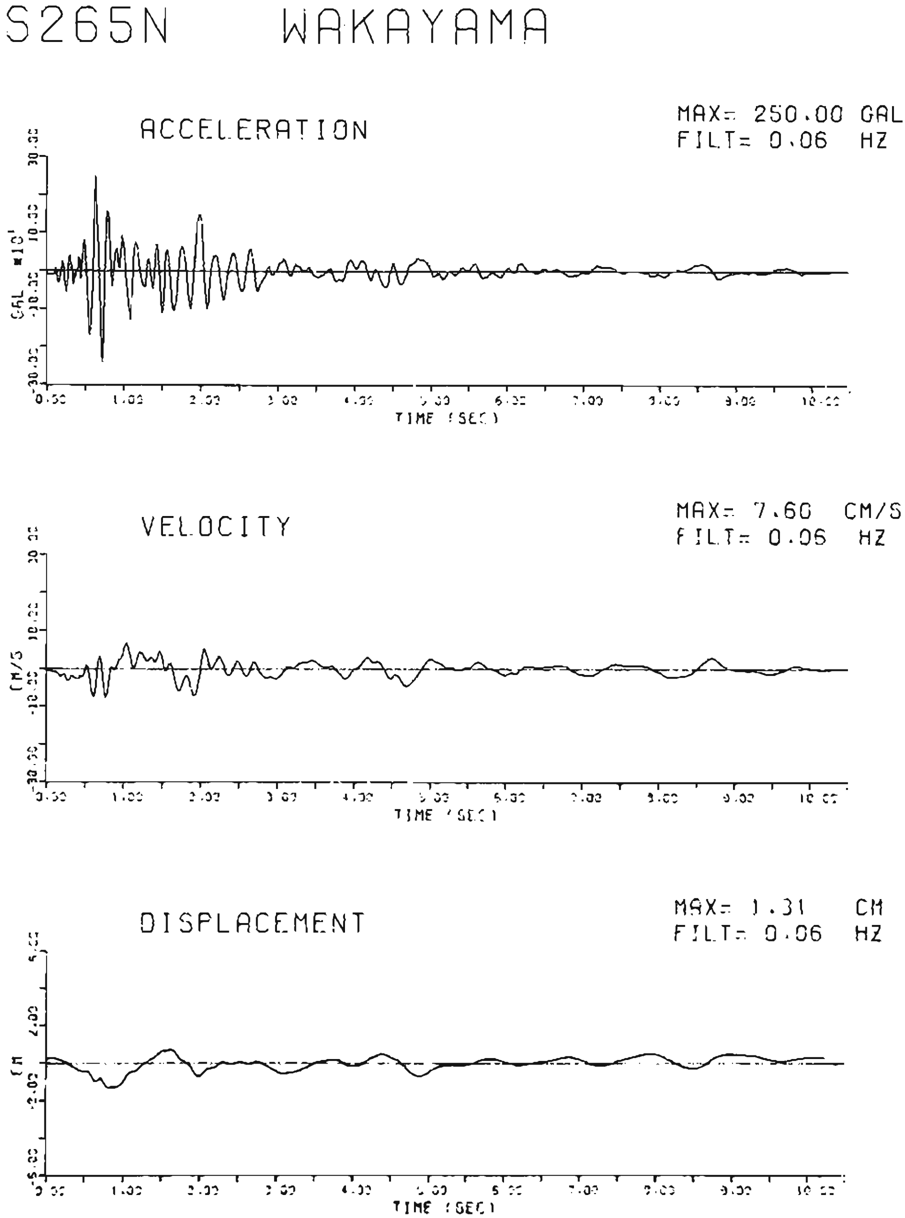
S265N WAKAYAMA
ACCELERATION
MAX= 250.00 GAL
FILT= 0.06 HZ
GAL *10¹
TIME (SEC)
VELOCITY
MAX= 7.60 CM/S
FILT= 0.06 HZ
CM/S
TIME (SEC)
DISPLACEMENT
MAX= 1.31 CM
FILT= 0.06 HZ
CM
TIME (SEC)

Fig. A-1

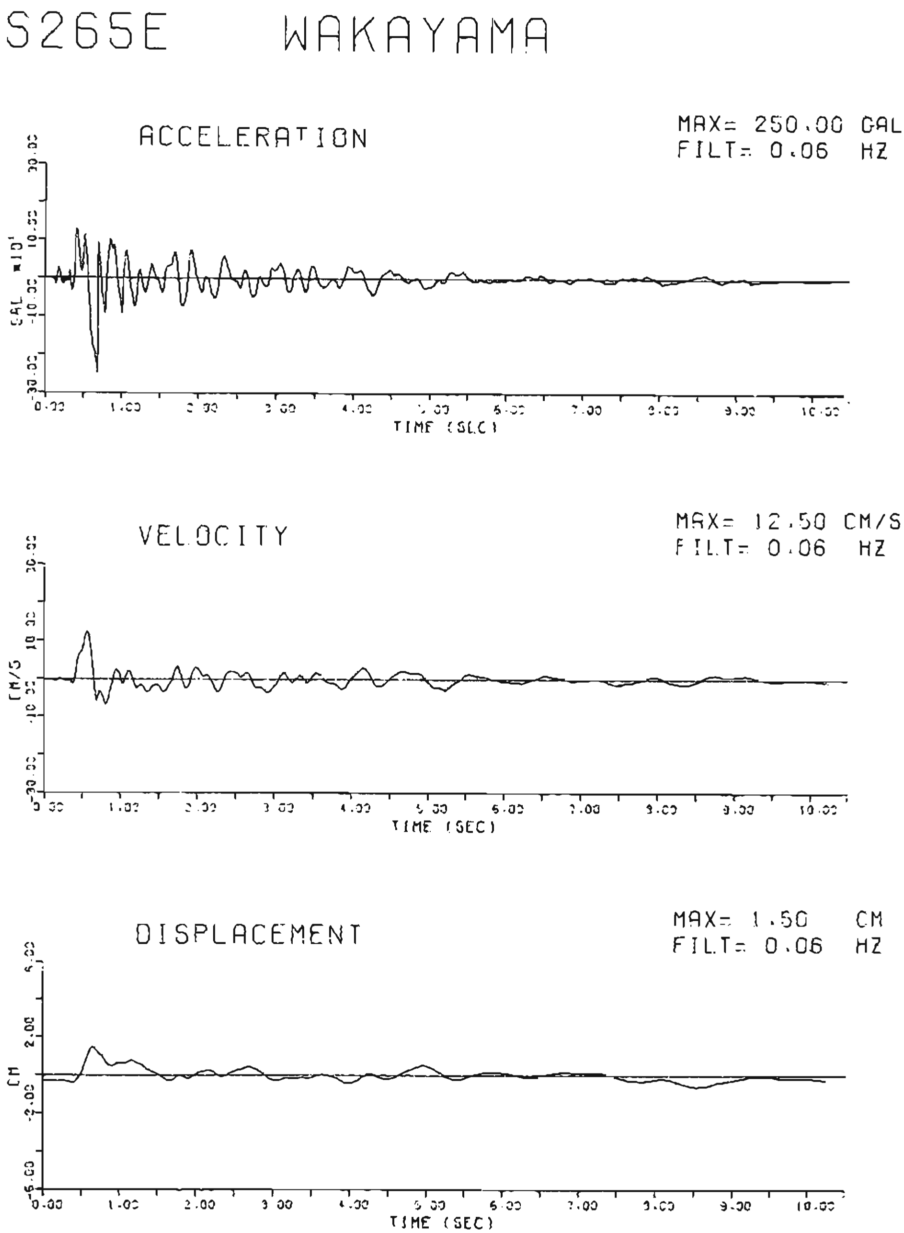
S265E WAKAYAMA
ACCELERATION
MAX= 250.00 GAL
FILT= 0.06 HZ
TIME (SEC)
VELOCITY
MAX= 12.50 CM/S
FILT= 0.06 HZ
CM/S
TIME (SEC)
DISPLACEMENT
MAX= 1.50 CM
FILT= 0.06 HZ
CM
TIME (SEC)

Fig. A-2

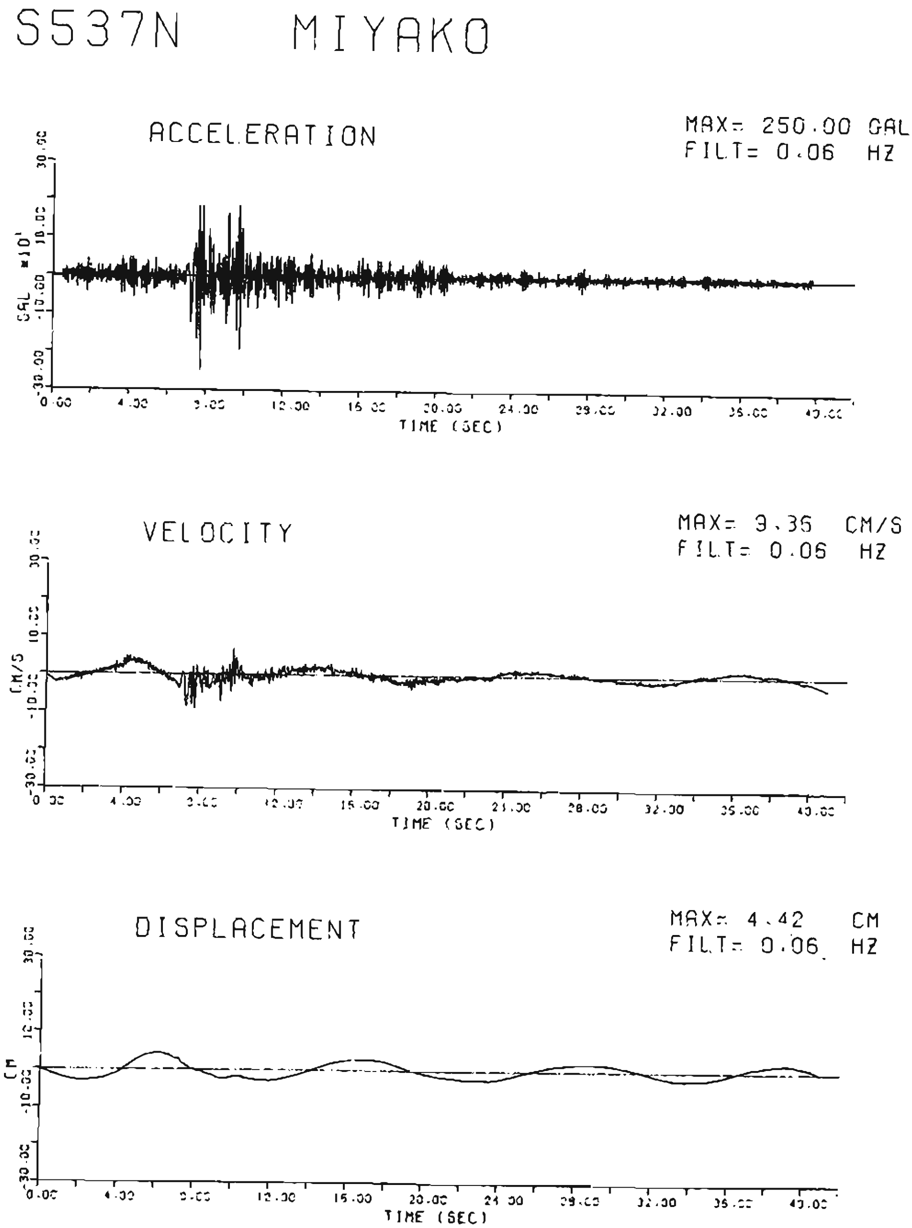
S537N MIYAKO
ACCELERATION
MAX= 250.00 GAL
FILT= 0.06 HZ
TIME (SEC)
VELOCITY
MAX= 9.35 CM/S
FILT= 0.06 HZ
CM/S
TIME (SEC)
DISPLACEMENT
MAX= 4.42 CM
FILT= 0.06 HZ
CM
TIME (SEC)

Fig. A-3

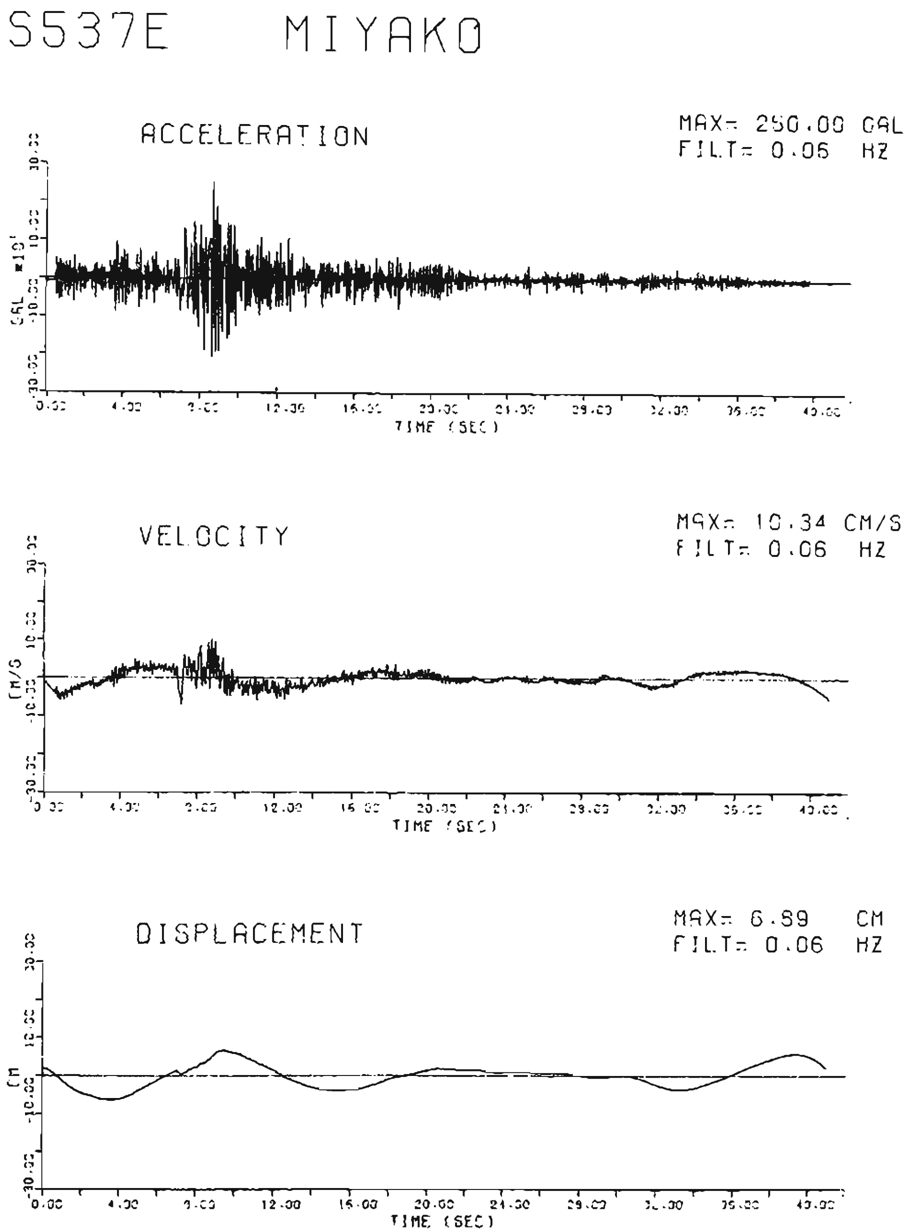
S537E MIYAKO
ACCELERATION
MAX= 250.00 GAL
FILT= 0.06 HZ
TIME (SEC)
VELOCITY
MAX= 10.34 CM/S
FILT= 0.06 HZ
TIME (SEC)
DISPLACEMENT
MAX= 6.89 CM
FILT= 0.06 HZ
TIME (SEC)

Fig. A-4

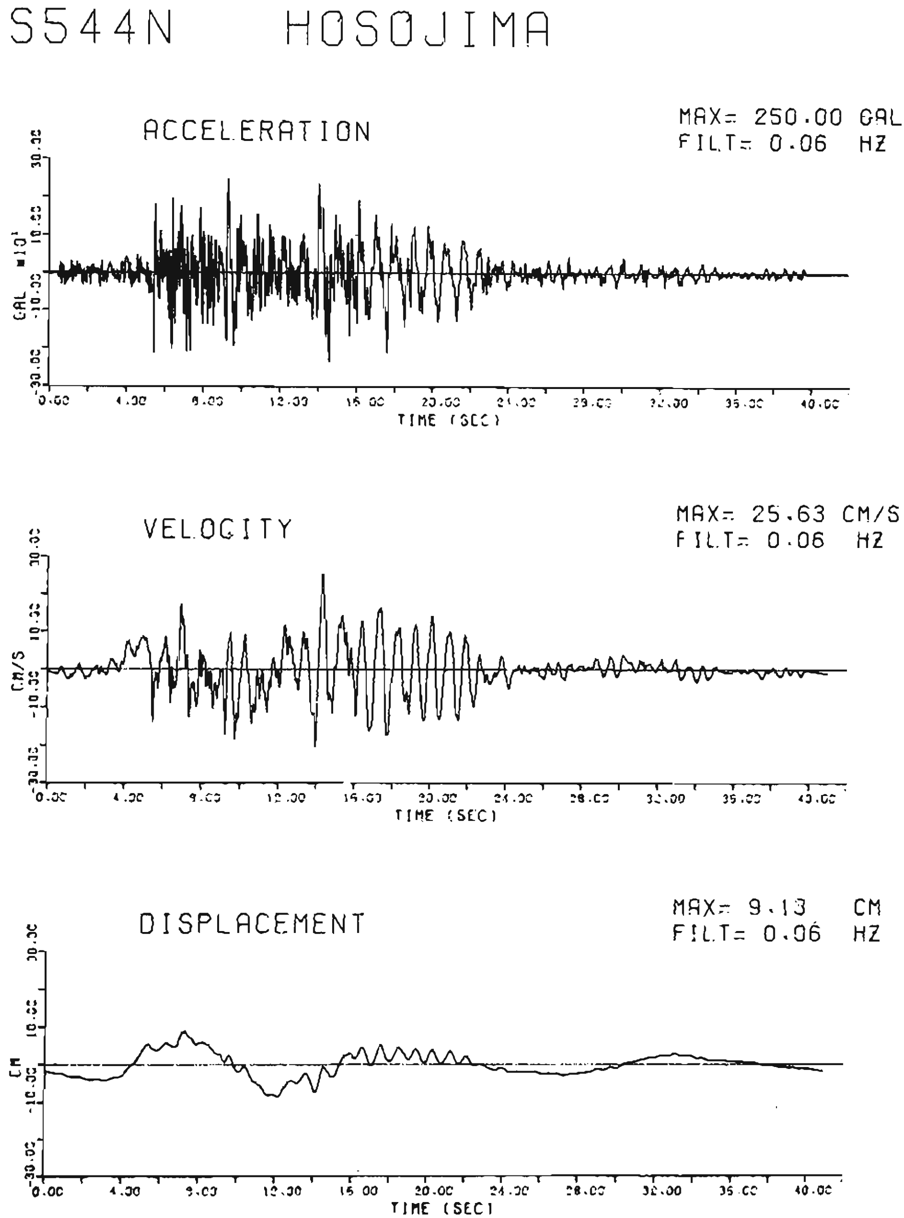
S544N HOSOJIMA
ACCELERATION
MAX= 250.00 GAL
FILT= 0.06 HZ
CAL ×10¹
TIME (SEC)
VELOCITY
MAX= 25.63 CM/S
FILT= 0.06 HZ
CM/S
TIME (SEC)
DISPLACEMENT
MAX= 9.13 CM
FILT= 0.06 HZ
CM
TIME (SEC)

Fig. A-5

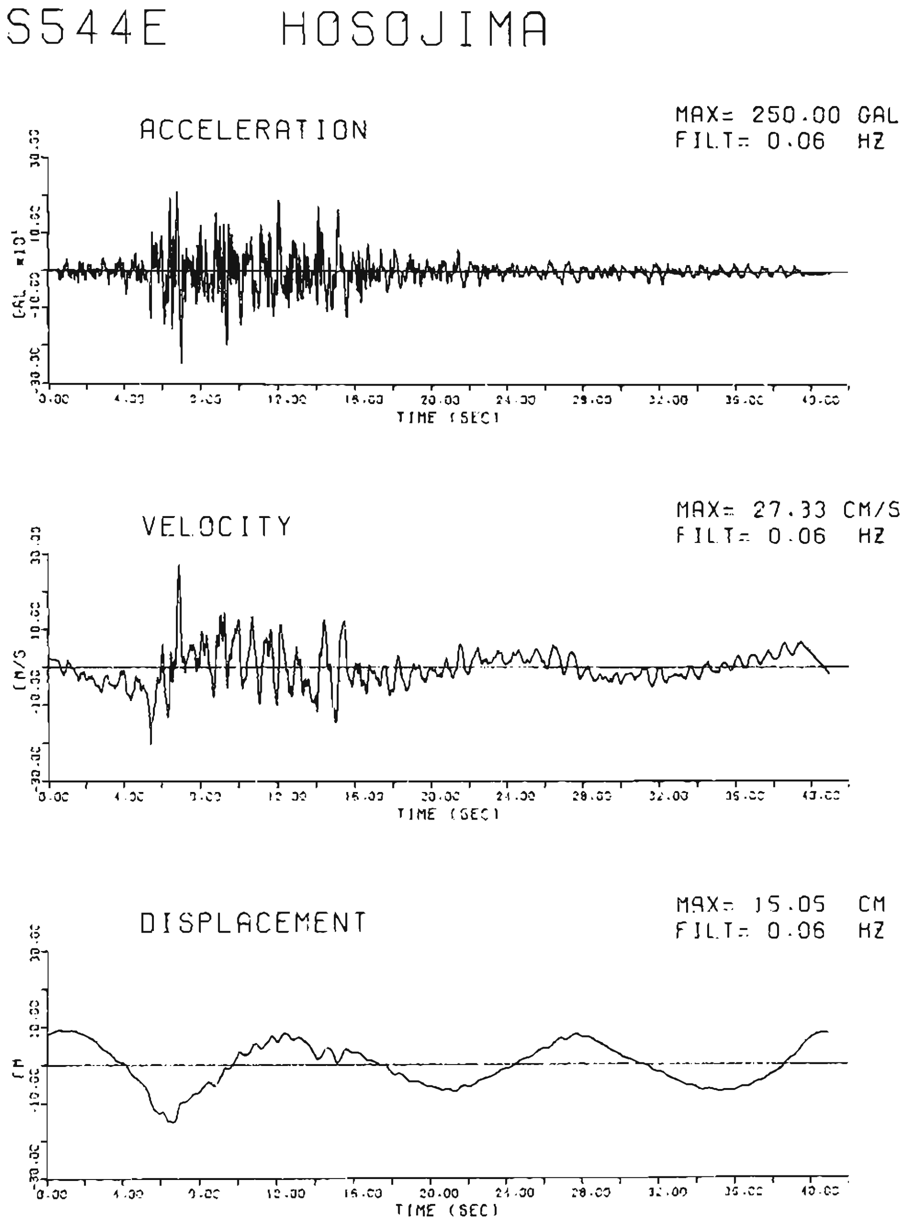
S544E HOSOJIMA
ACCELERATION
MAX= 250.00 GAL
FILT= 0.06 HZ
TIME (SEC)
VELOCITY
MAX= 27.33 CM/S
FILT= 0.06 HZ
TIME (SEC)
DISPLACEMENT
MAX= 15.05 CM
FILT= 0.06 HZ
TIME (SEC)

Fig. A-6

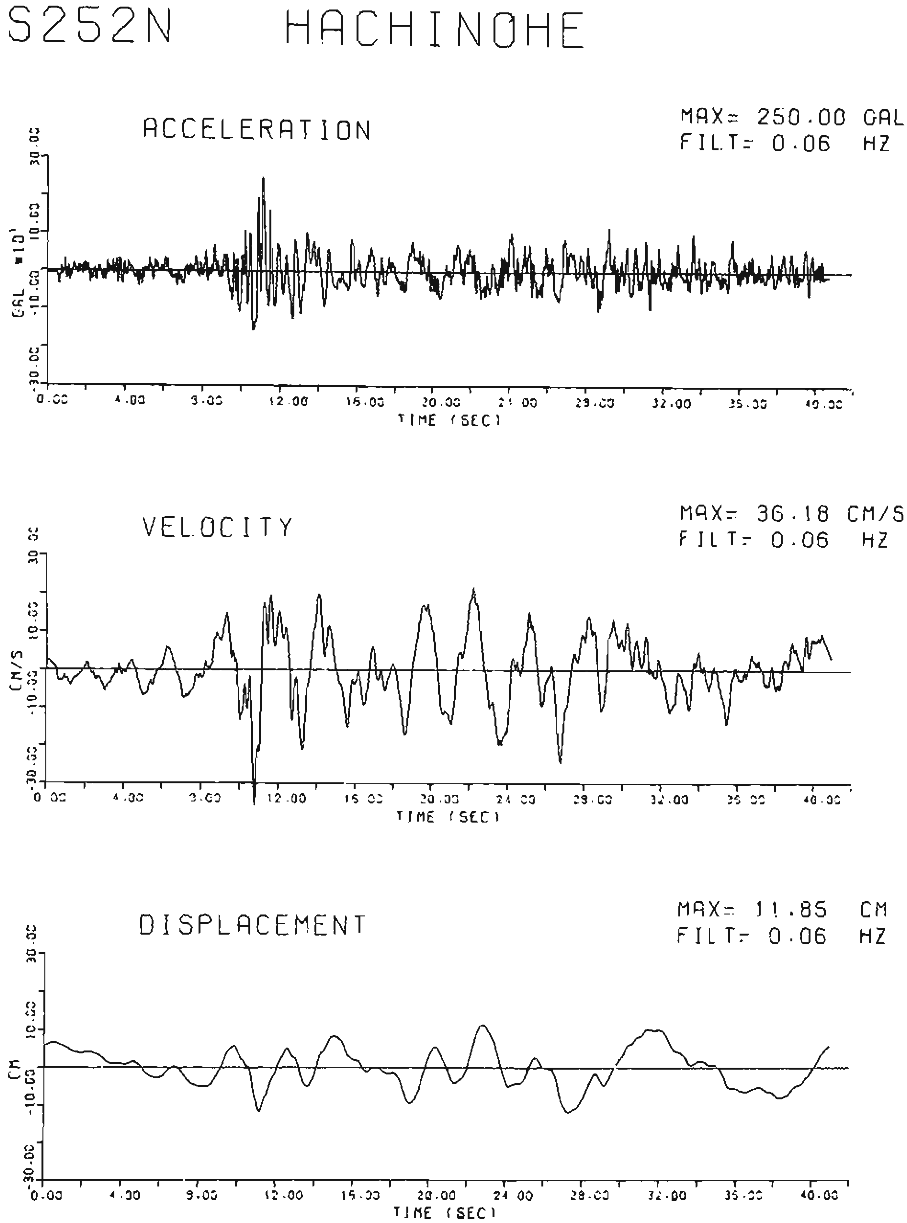
S252N HACHINOHE
ACCELERATION
MAX= 250.00 GAL
FILT= 0.06 HZ
GAL *10¹
TIME (SEC)
VELOCITY
MAX= 36.18 CM/S
FILT= 0.06 HZ
CM/S
TIME (SEC)
DISPLACEMENT
MAX= 11.85 CM
FILT= 0.06 HZ
CM
TIME (SEC)

Fig. A-7

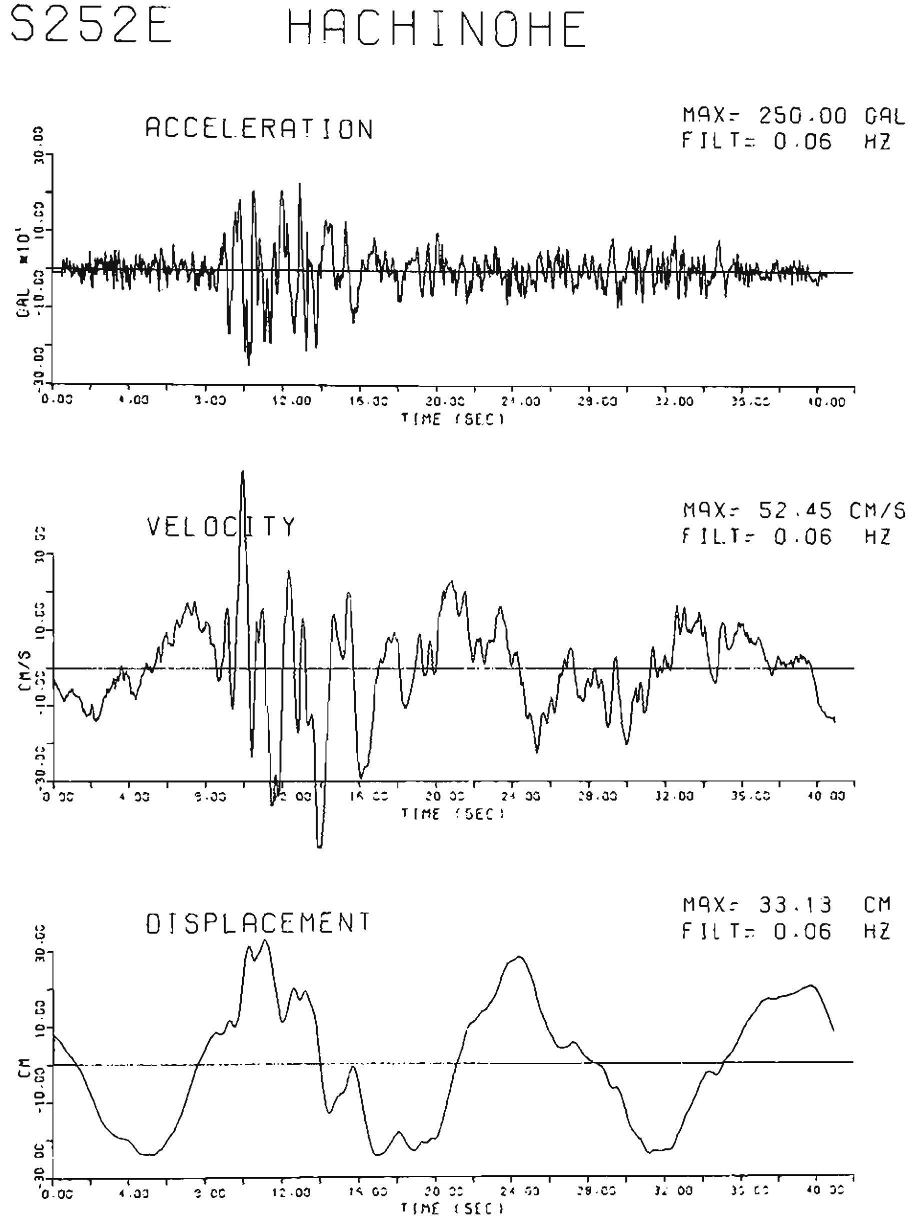
S252E HACHINOHE
ACCELERATION
MAX= 250.00 GAL
FILT= 0.06 HZ
GAL ×10'
TIME (SEC)
VELOCITY
MAX= 52.45 CM/S
FILT= 0.06 HZ
CM/S
TIME (SEC)
DISPLACEMENT
MAX= 33.13 CM
FILT= 0.06 HZ
CM
TIME (SEC)

Fig. A-8

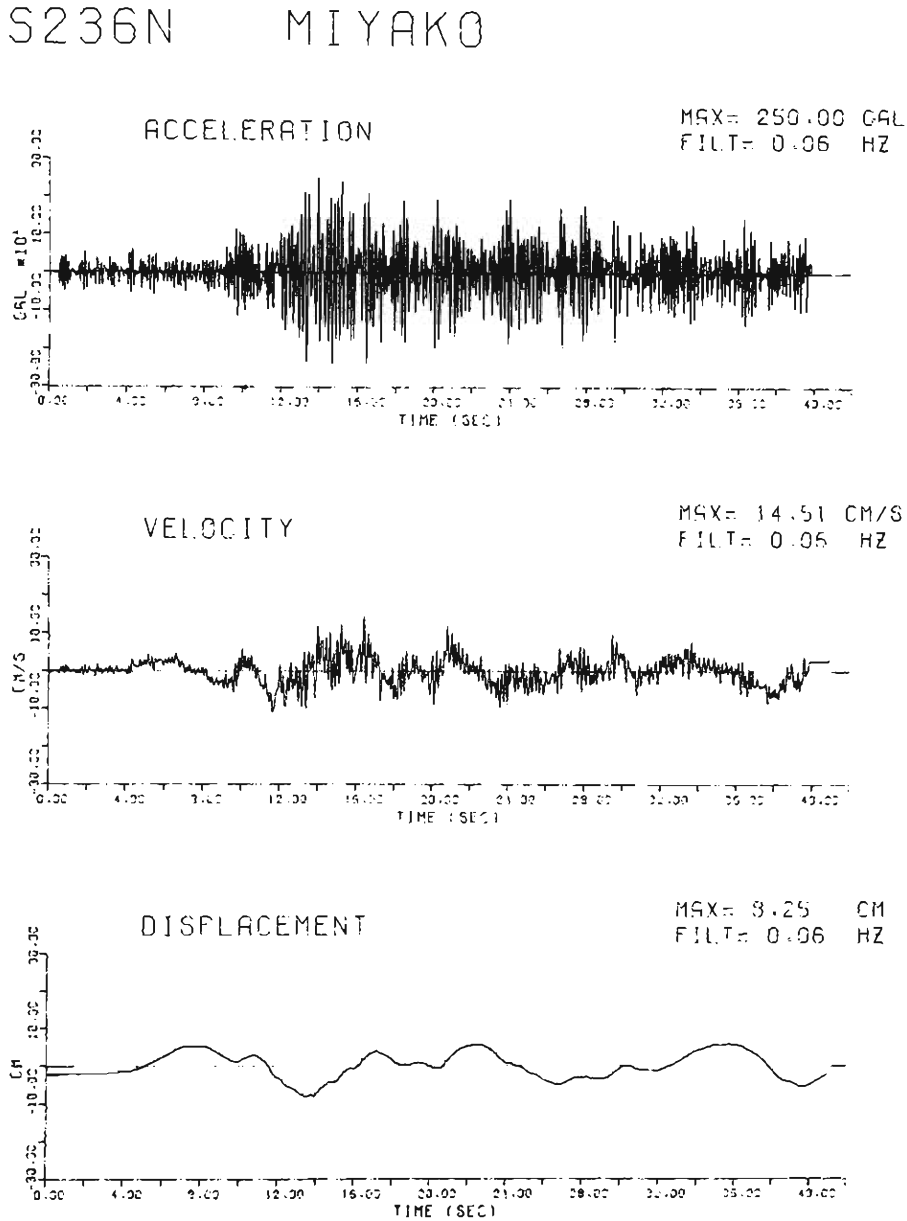
S236N MIYAKO
ACCELERATION
MAX= 250.00 GAL
FILT= 0.06 HZ
TIME (SEC)
VELOCITY
MAX= 14.51 CM/S
FILT= 0.06 HZ
CM/S
TIME (SEC)
DISPLACEMENT
MAX= 8.25 CM
FILT= 0.06 HZ
CM
TIME (SEC)

Fig. A-9

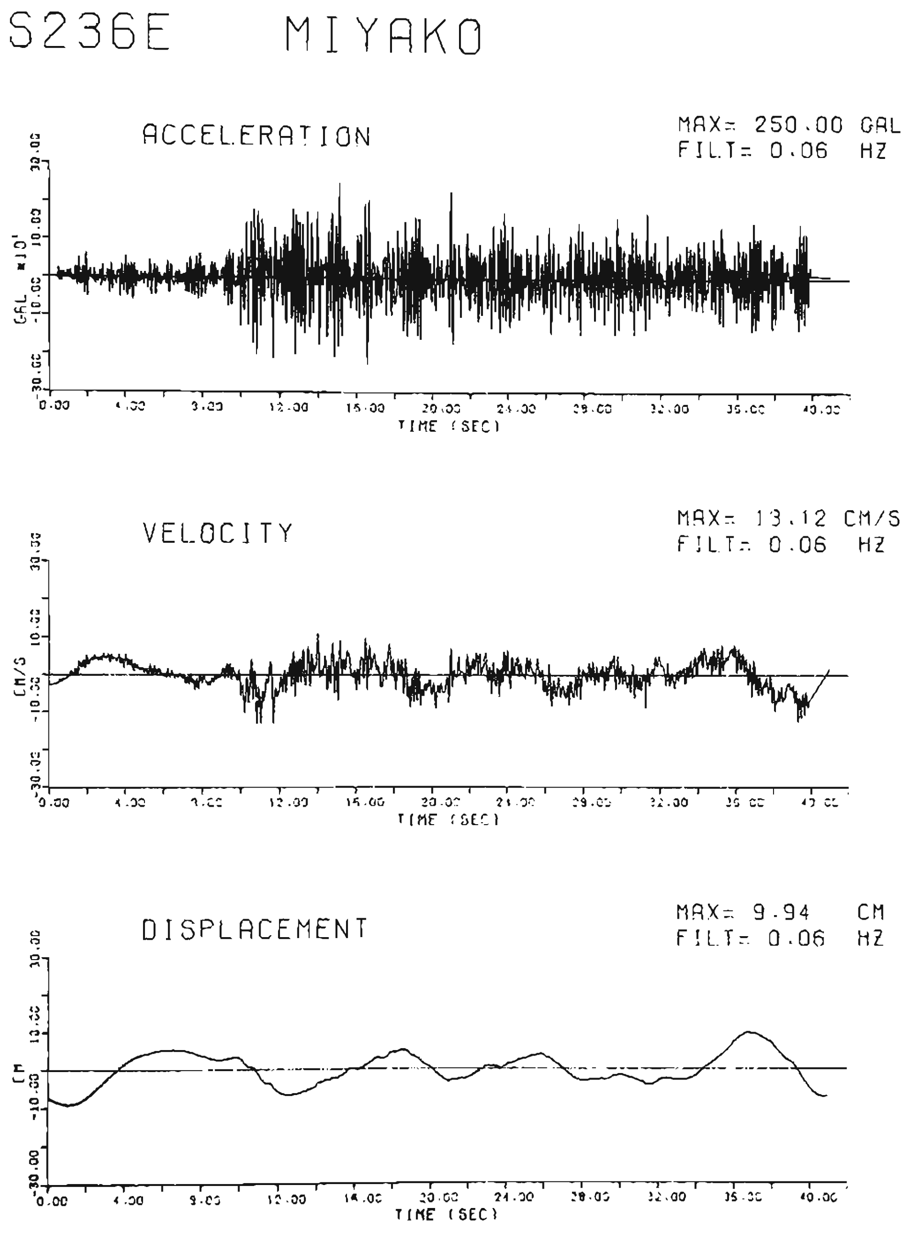
S236E MIYAKO
ACCELERATION
MAX= 250.00 GAL
FILT= 0.06 HZ
TIME (SEC)
VELOCITY
MAX= 13.12 CM/S
FILT= 0.06 HZ
CM/S
DISPLACEMENT
MAX= 9.94 CM
FILT= 0.06 HZ
CM
TIME (SEC)

Fig. A-10

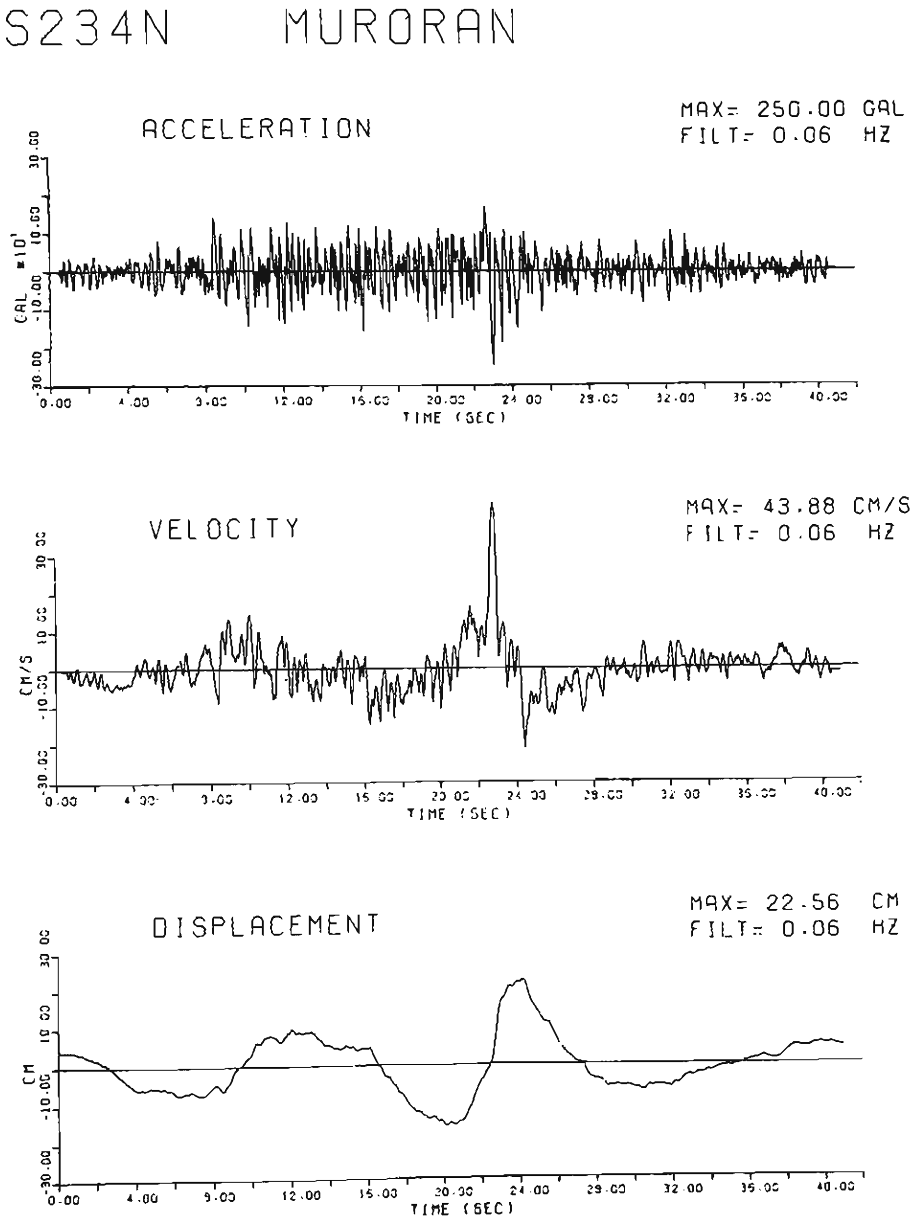
S234N MURORAN
ACCELERATION
MAX= 250.00 GAL
FILT= 0.06 HZ
TIME (SEC)
VELOCITY
MAX= 43.88 CM/S
FILT= 0.06 HZ
CM/S
TIME (SEC)
DISPLACEMENT
MAX= 22.56 CM
FILT= 0.06 HZ
CM
TIME (SEC)

Fig. A-11

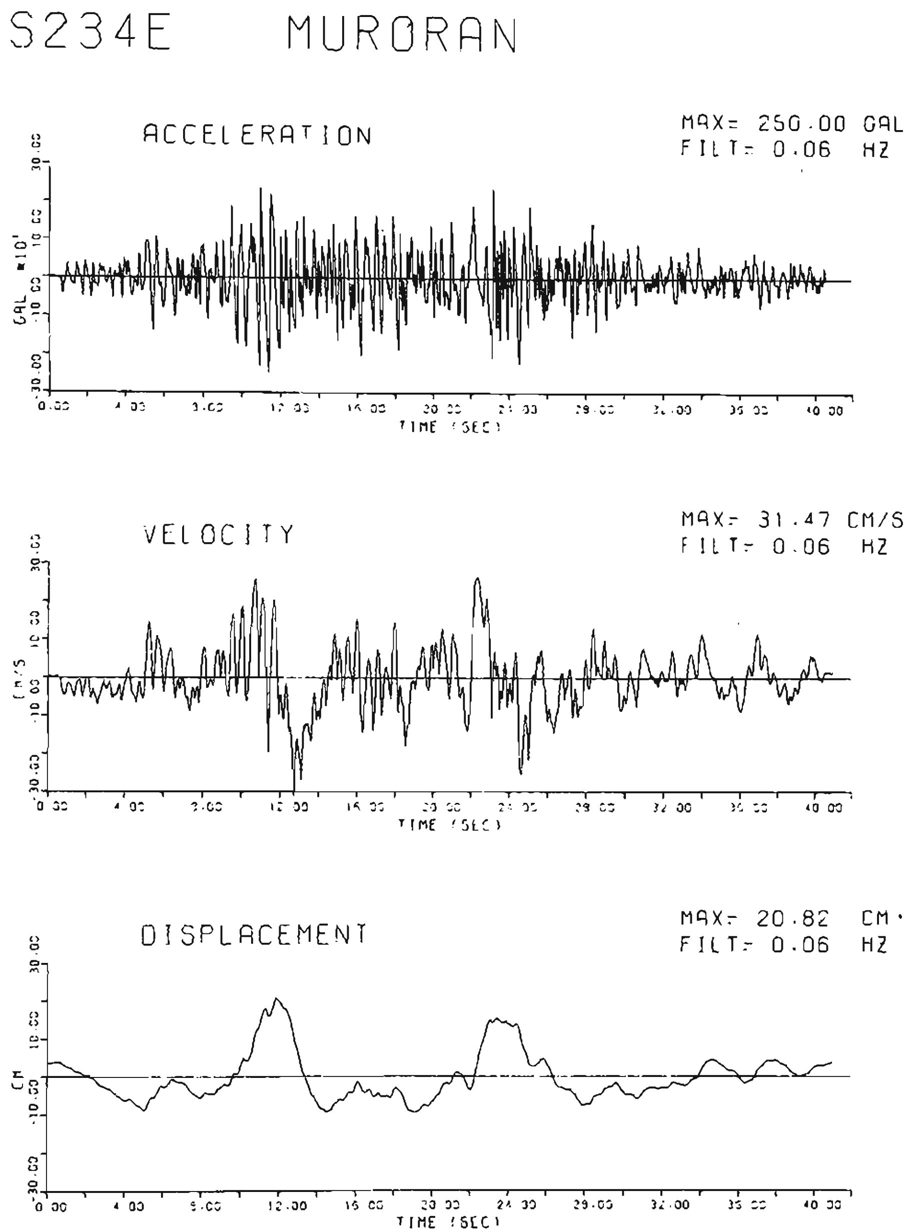
S234E MURORAN
ACCELERATION
MAX= 250.00 GAL
FILT= 0.06 HZ
GAL
TIME (SEC)
VELOCITY
MAX= 31.47 CM/S
FILT= 0.06 HZ
TIME (SEC)
DISPLACEMENT
MAX= 20.82 CM
FILT= 0.06 HZ
CM
TIME (SEC)

Fig. A-12

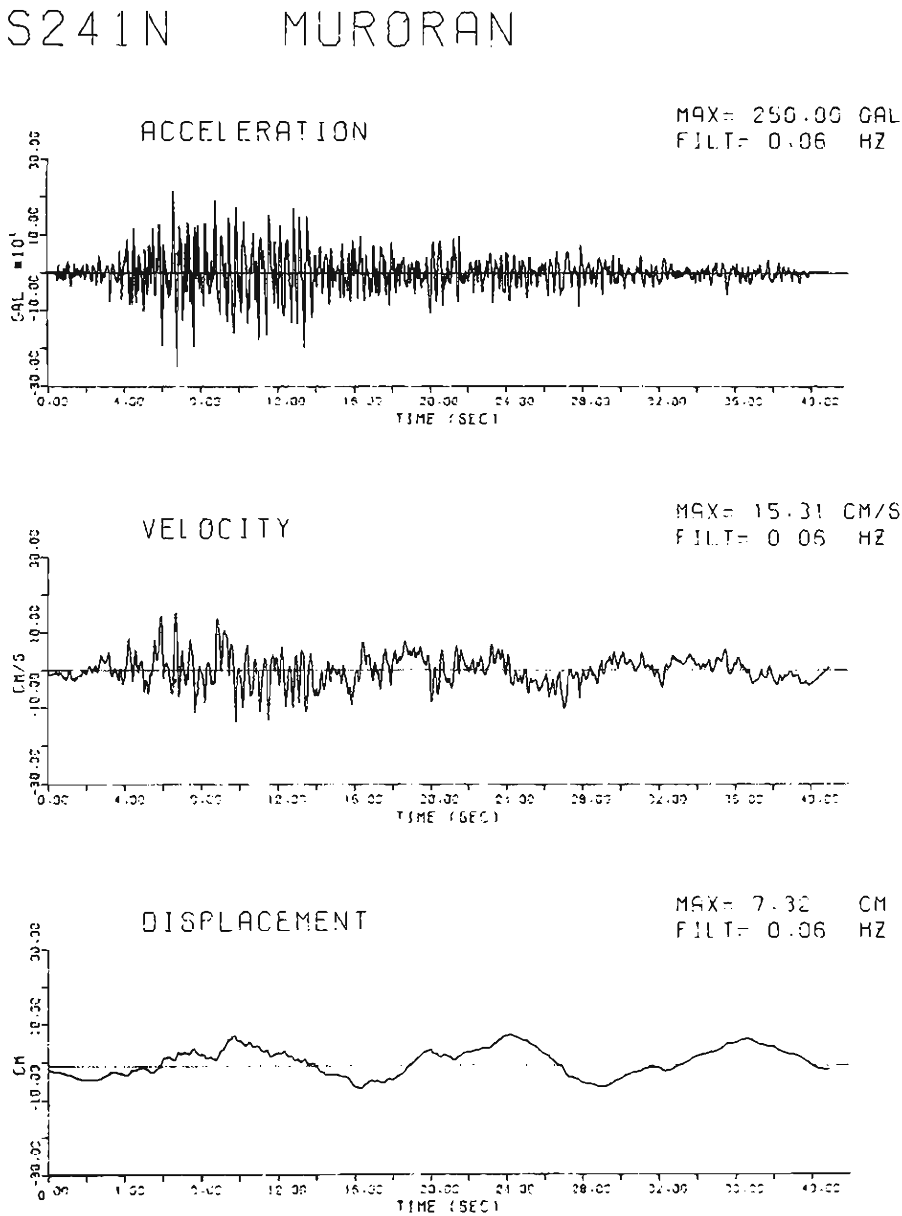
S241N MURORAN
ACCELERATION
MAX= 250.00 GAL
FILT= 0.06 HZ
TIME (SEC)
VELOCITY
MAX= 15.31 CM/S
FILT= 0.06 HZ
CM/S
DISPLACEMENT
MAX= 7.32 CM
FILT= 0.06 HZ
CM
TIME (SEC)

Fig. A-13

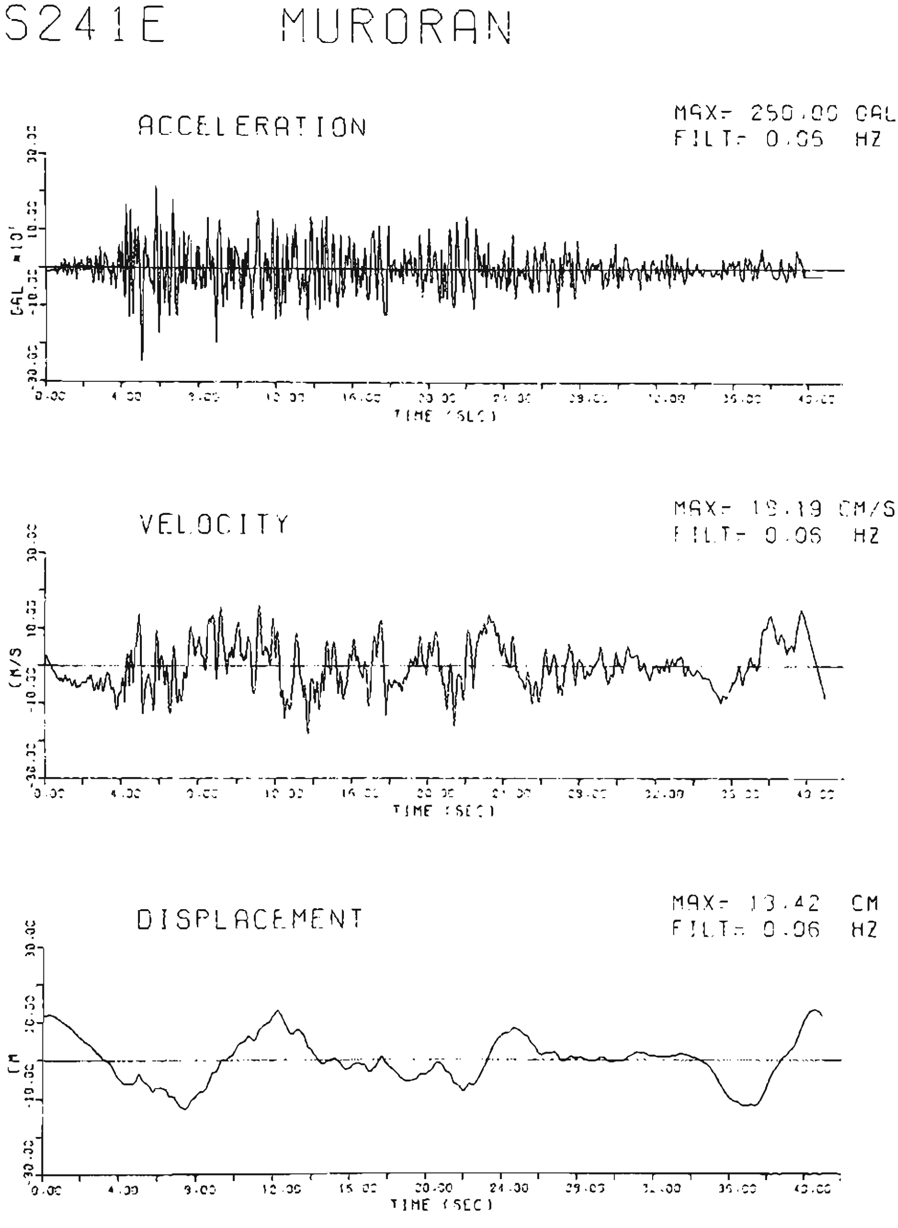
S241E MURORAN
ACCELERATION
MAX= 250.00 GAL
FILT= 0.05 HZ
TIME (SEC)
VELOCITY
FILT= 0.06 HZ
CM/S
TIME (SEC)
DISPLACEMENT
MAX= 13.42 CM
FILT= 0.06 HZ
CM
TIME (SEC)

Fig. A-14

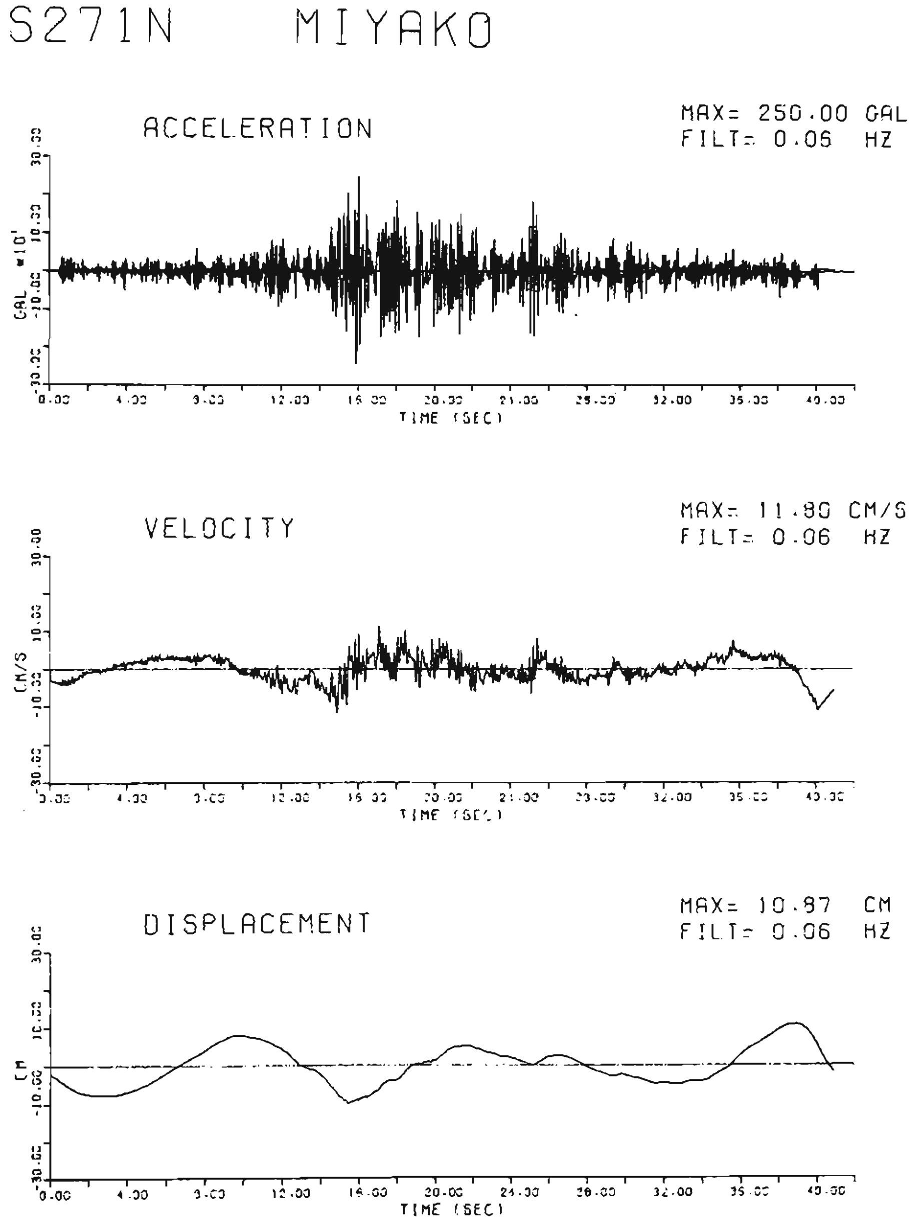
S271N MIYAKO
ACCELERATION
MAX= 250.00 GAL
FILT= 0.06 HZ
GAL *10'
TIME (SEC)
VELOCITY
MAX= 11.80 CM/S
FILT= 0.06 HZ
CM/S
DISPLACEMENT
MAX= 10.87 CM
FILT= 0.06 HZ
CM
TIME (SEC)

Fig. A-15

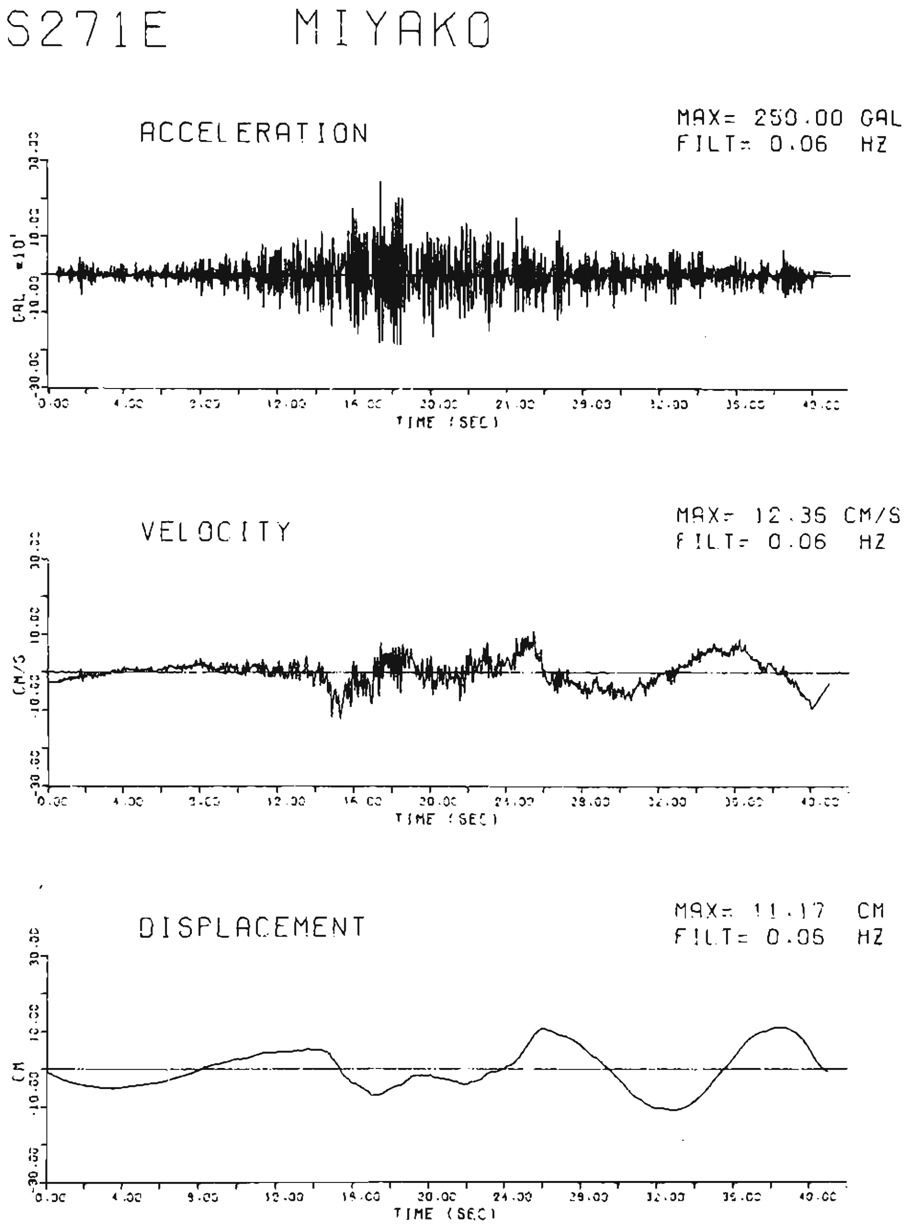
S271E MIYAKO
ACCELERATION
MAX= 250.00 GAL
FILT= 0.06 HZ
TIME (SEC)
VELOCITY
MAX= 12.36 CM/S
FILT= 0.06 HZ
CM/S
TIME (SEC)
DISPLACEMENT
MAX= 11.17 CM
FILT= 0.06 HZ
CM
TIME (SEC)

Fig. A-16

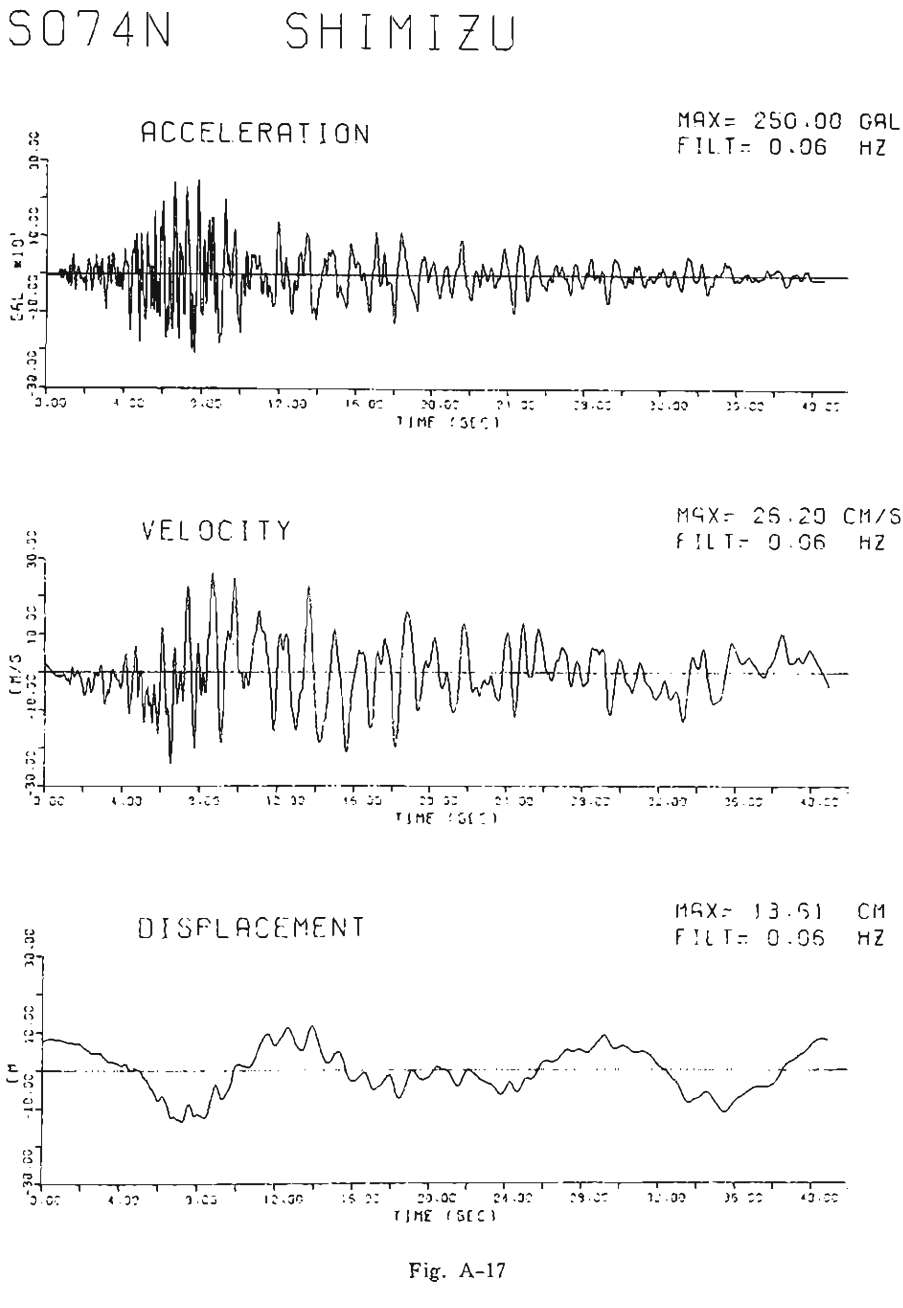
S074N SHIMIZU
ACCELERATION
MAX= 250.00 GAL
FILT= 0.06 HZ
VELOCITY
MAX= 26.20 CM/S
FILT= 0.06 HZ
DISPLACEMENT
MAX= 13.61 CM
FILT= 0.06 HZ
TIME (SEC)

Fig. A-17

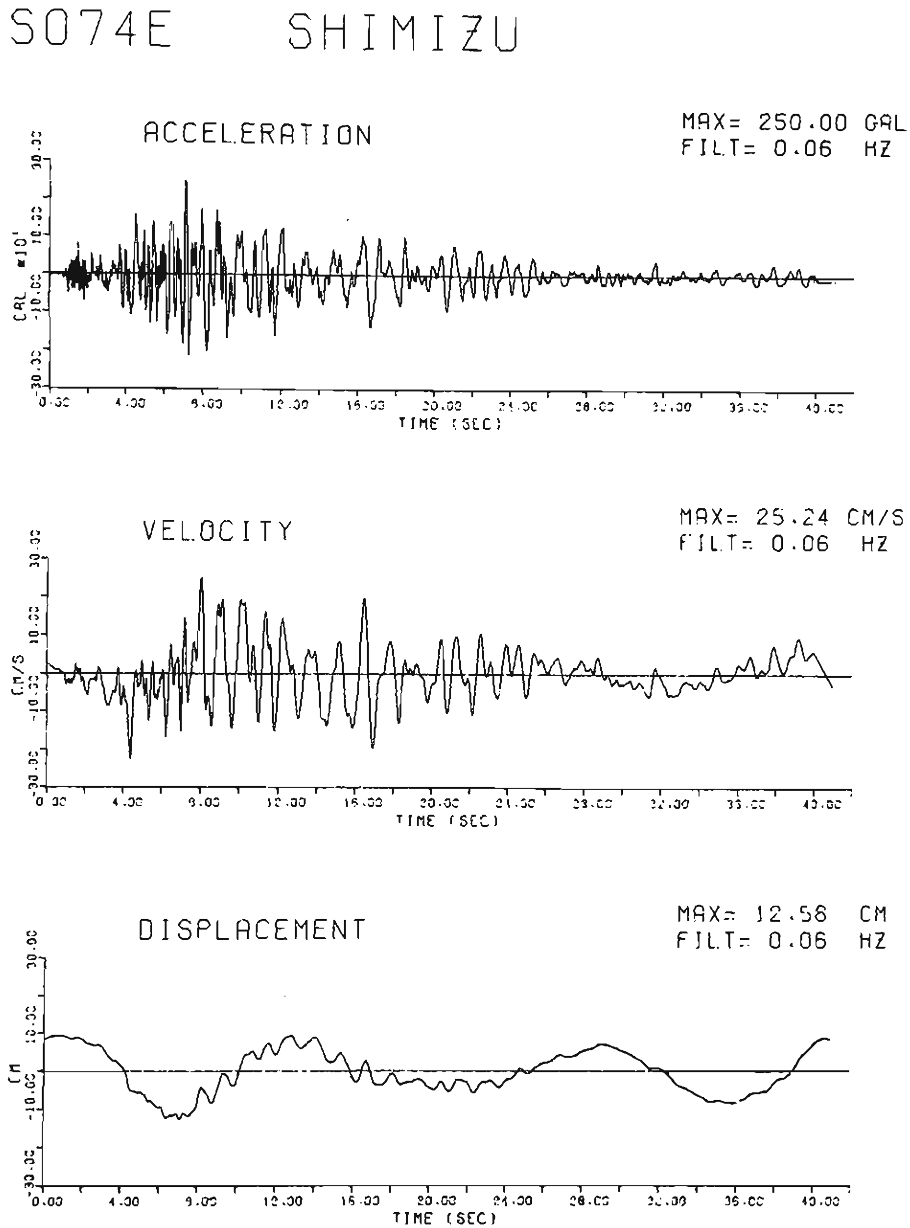
S074E SHIMIZU
ACCELERATION
MAX= 250.00 GAL
FILT= 0.06 HZ
TIME (SEC)
VELOCITY
MAX= 25.24 CM/S
FILT= 0.06 HZ
CM/S
TIME (SEC)
DISPLACEMENT
MAX= 12.58 CM
FILT= 0.06 HZ
CM
TIME (SEC)

Fig. A–18

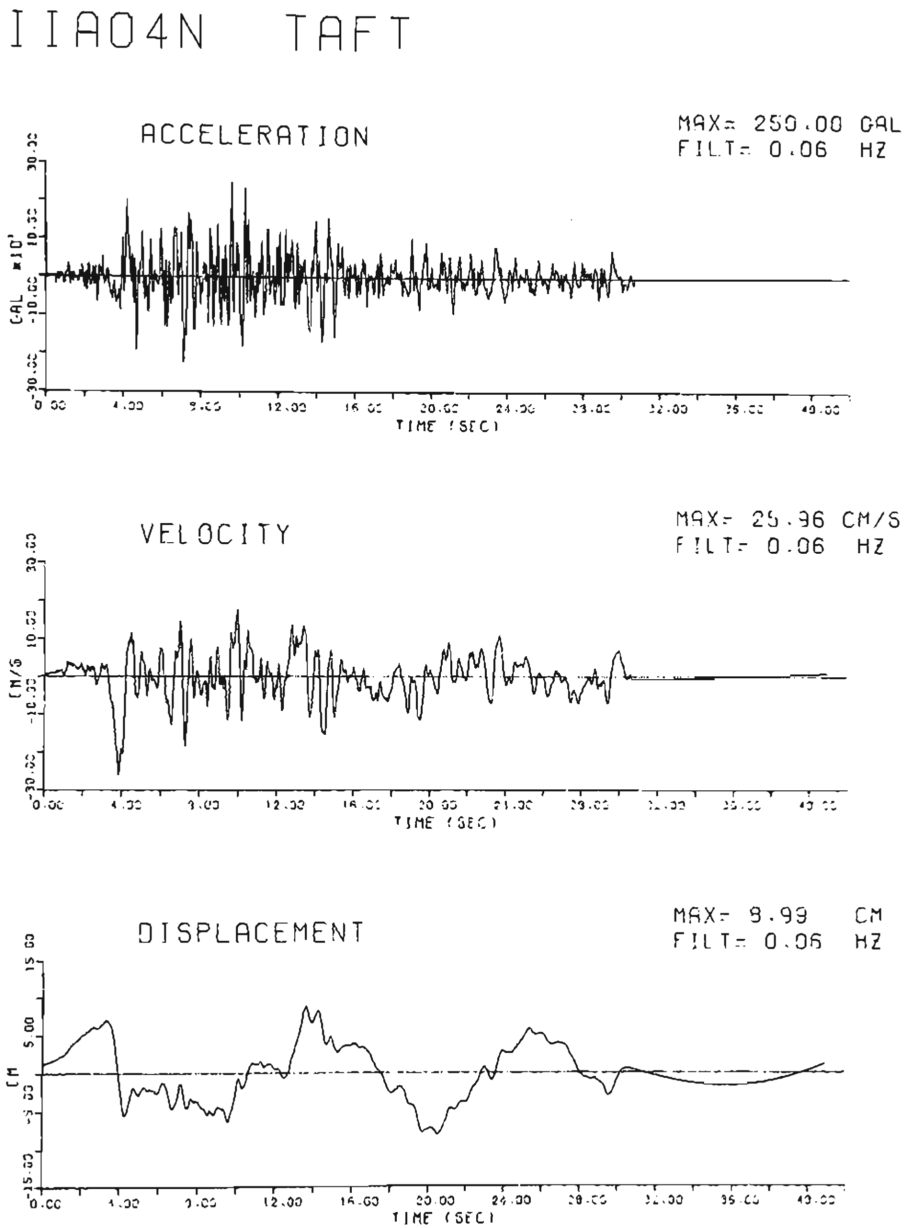
IIA04N TAFT
ACCELERATION
MAX= 250.00 GAL
FILT= 0.06 HZ
GAL x10'
TIME (SEC)
VELOCITY
MAX= 25.96 CM/S
FILT= 0.06 HZ
CM/S
TIME (SEC)
DISPLACEMENT
MAX= 8.99 CM
FILT= 0.06 HZ
CM
TIME (SEC)

Fig. A-19

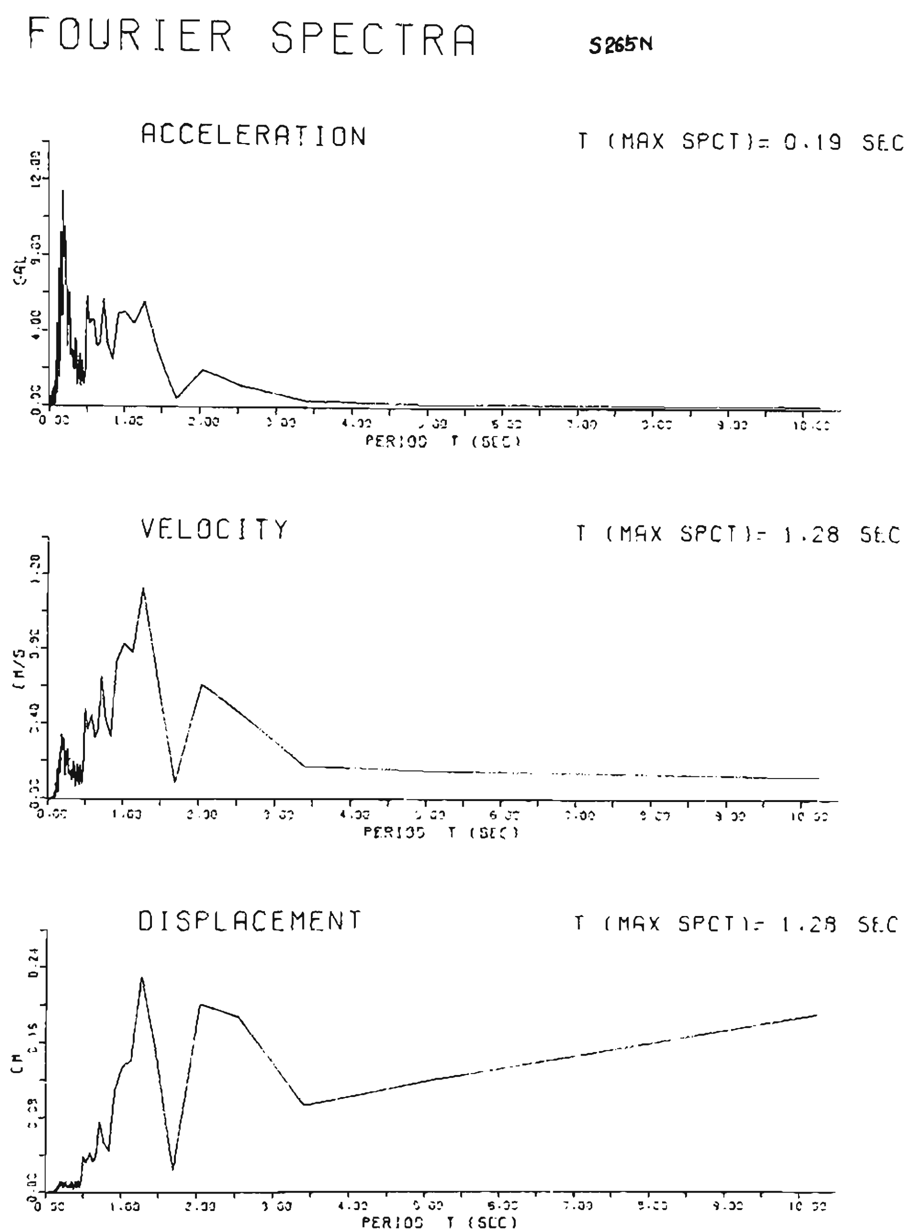
FOURIER SPECTRA
S265N
ACCELERATION
T (MAX SPCT)= 0.19 SEC
GAL
PERIOD T (SEC)
VELOCITY
T (MAX SPCT)= 1.28 SEC
CM/S
PERIOD T (SEC)
DISPLACEMENT
T (MAX SPCT)= 1.28 SEC
CM
PERIOD T (SEC)

Fig. A-20

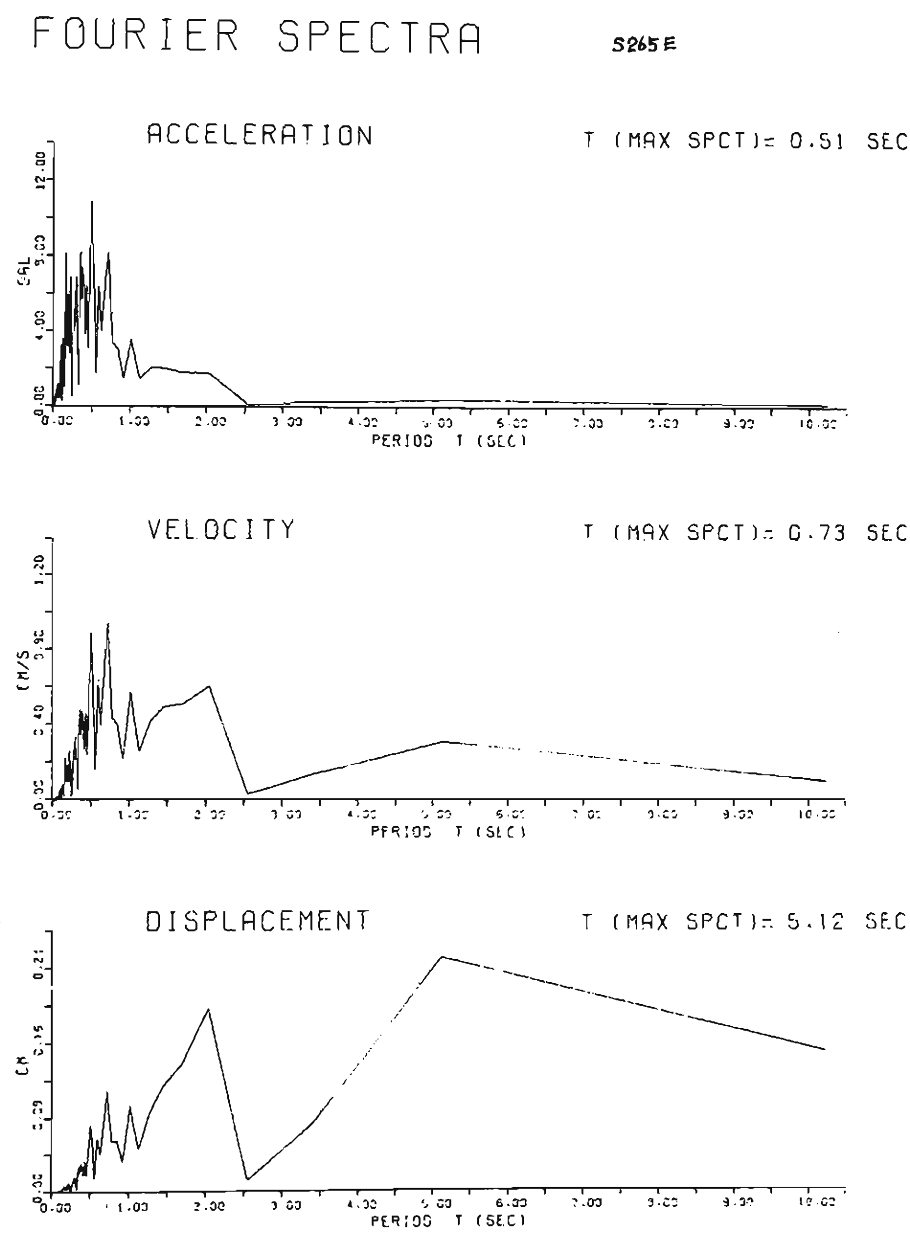

FOURIER SPECTRA
S265E
ACCELERATION
T (MAX SPCT)= 0.51 SEC
GAL
PERIOD T (SEC)
VELOCITY
T (MAX SPCT)= 0.73 SEC
CM/S
PERIOD T (SEC)
DISPLACEMENT
T (MAX SPCT)= 5.12 SEC
CM
PERIOD T (SEC)

Fig. A-21

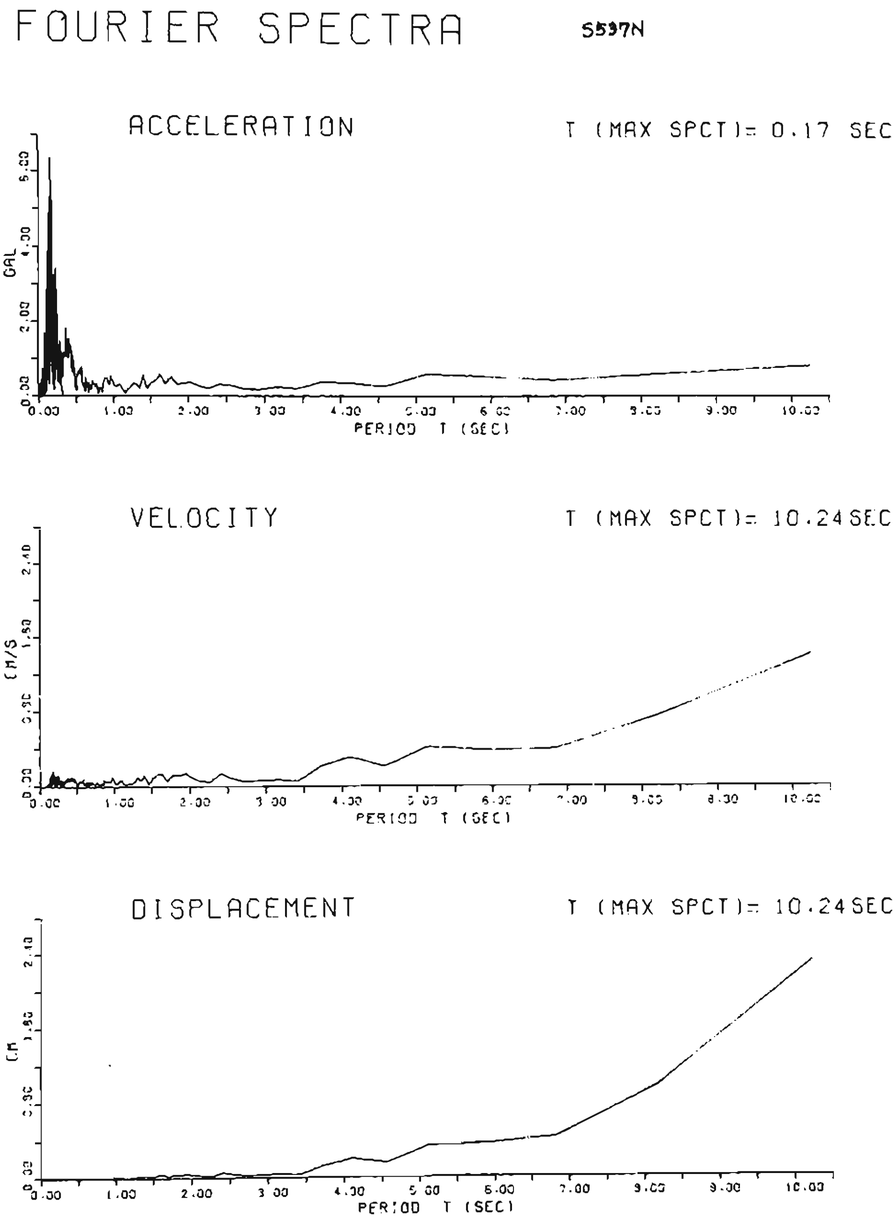
FOURIER SPECTRA
S537N
ACCELERATION
T (MAX SPCT)= 0.17 SEC
GAL
PERIOD T (SEC)
VELOCITY
T (MAX SPCT)= 10.24 SEC
CM/S
PERIOD T (SEC)
DISPLACEMENT
T (MAX SPCT)= 10.24 SEC
CM
PERIOD T (SEC)

Fig. A-22

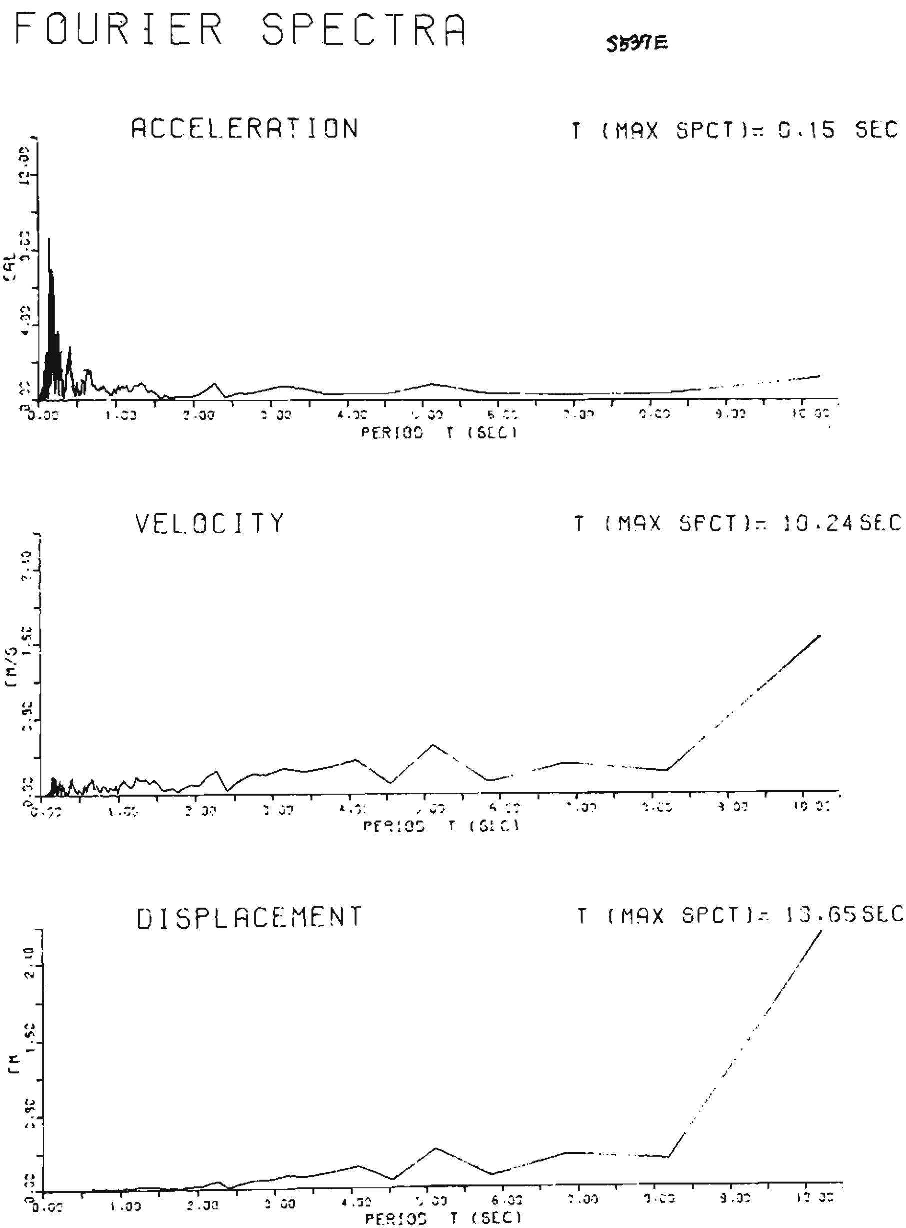
FOURIER SPECTRA
S537E
ACCELERATION
T (MAX SPCT)= 0.15 SEC
GAL
PERIOD T (SEC)
VELOCITY
T (MAX SPCT)= 10.24 SEC
CM/S
PERIOD T (SEC)
DISPLACEMENT
T (MAX SPCT)= 10.65 SEC
CM
PERIOD T (SEC)

Fig. A-23

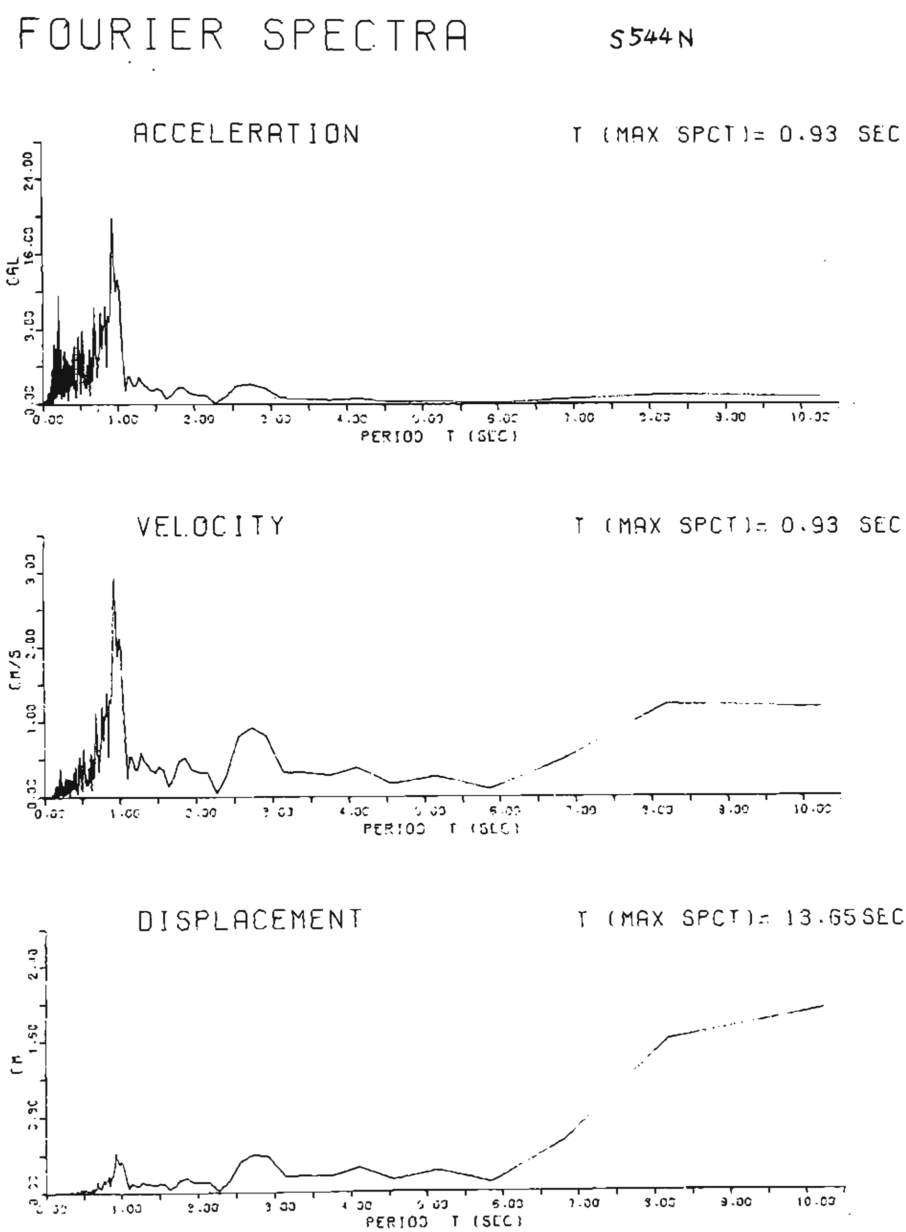
FOURIER SPECTRA
S544N
ACCELERATION
T (MAX SPCT)= 0.93 SEC
GAL
PERIOD T (SEC)
VELOCITY
T (MAX SPCT)= 0.93 SEC
CM/S
PERIOD T (SEC)
DISPLACEMENT
T (MAX SPCT)= 13.65 SEC
CM
PERIOD T (SEC)

Fig. A-24

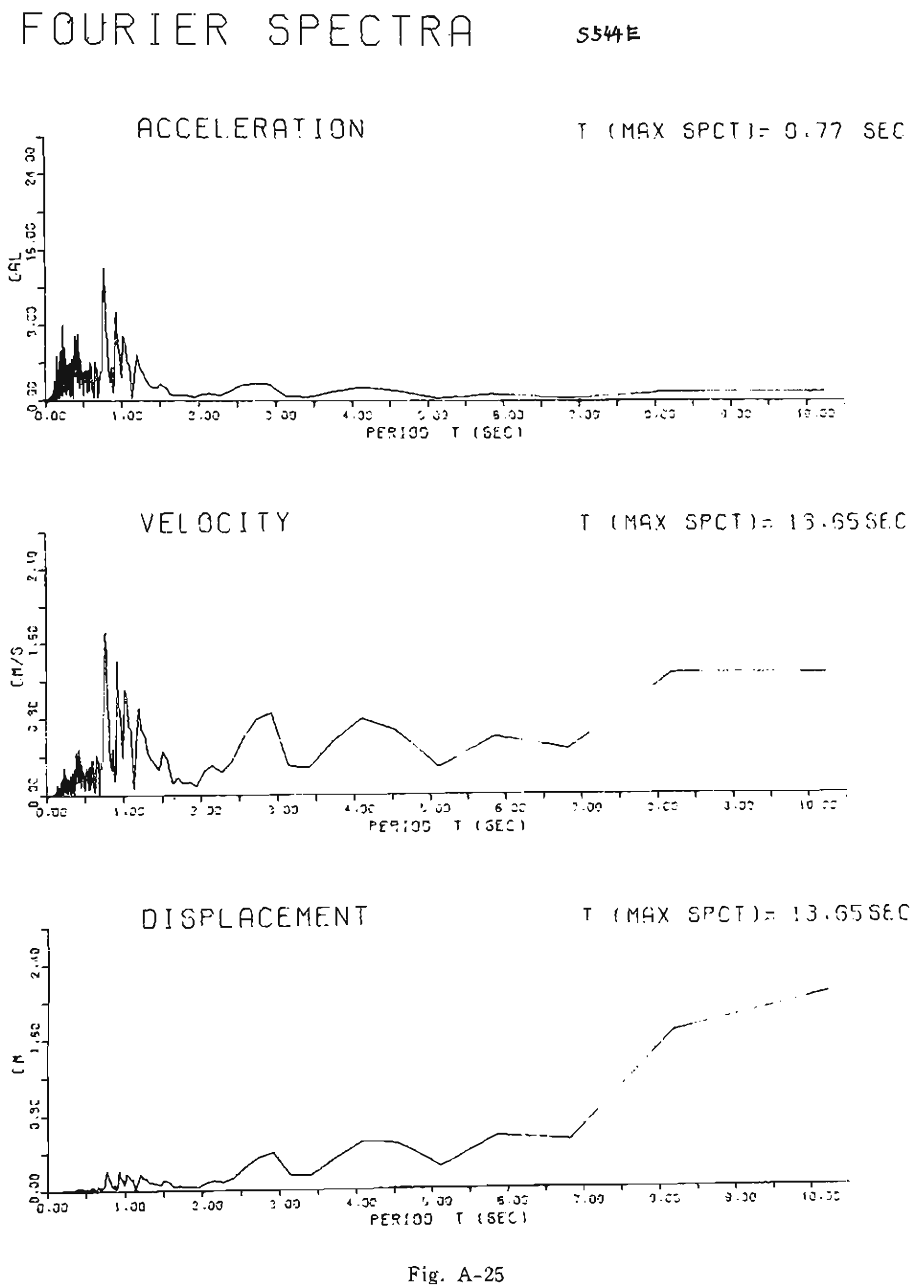

FOURIER SPECTRA
S544E
ACCELERATION
T (MAX SPCT)= 0.77 SEC
GAL
PERIOD T (SEC)
VELOCITY
T (MAX SPCT)= 13.65SEC
CM/S
PERIOD T (SEC)
DISPLACEMENT
T (MAX SPCT)= 13.65SEC
CM
PERIOD T (SEC)

Fig. A-25

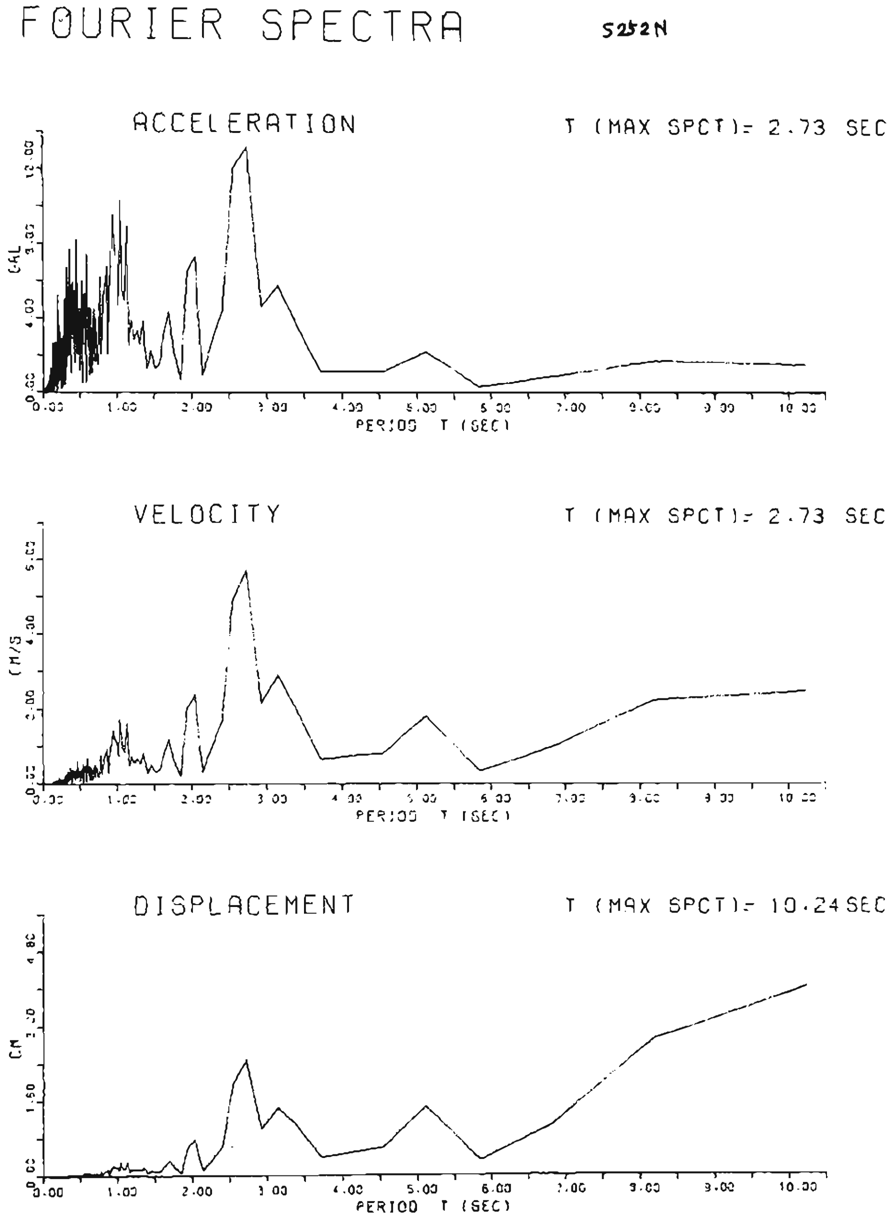
FOURIER SPECTRA
S252N
ACCELERATION
T (MAX SPCT)= 2.73 SEC
GAL
VELOCITY
T (MAX SPCT)= 2.73 SEC
CM/S
DISPLACEMENT
T (MAX SPCT)= 10.24 SEC
CM
PERIOD T (SEC)

Fig. A-26

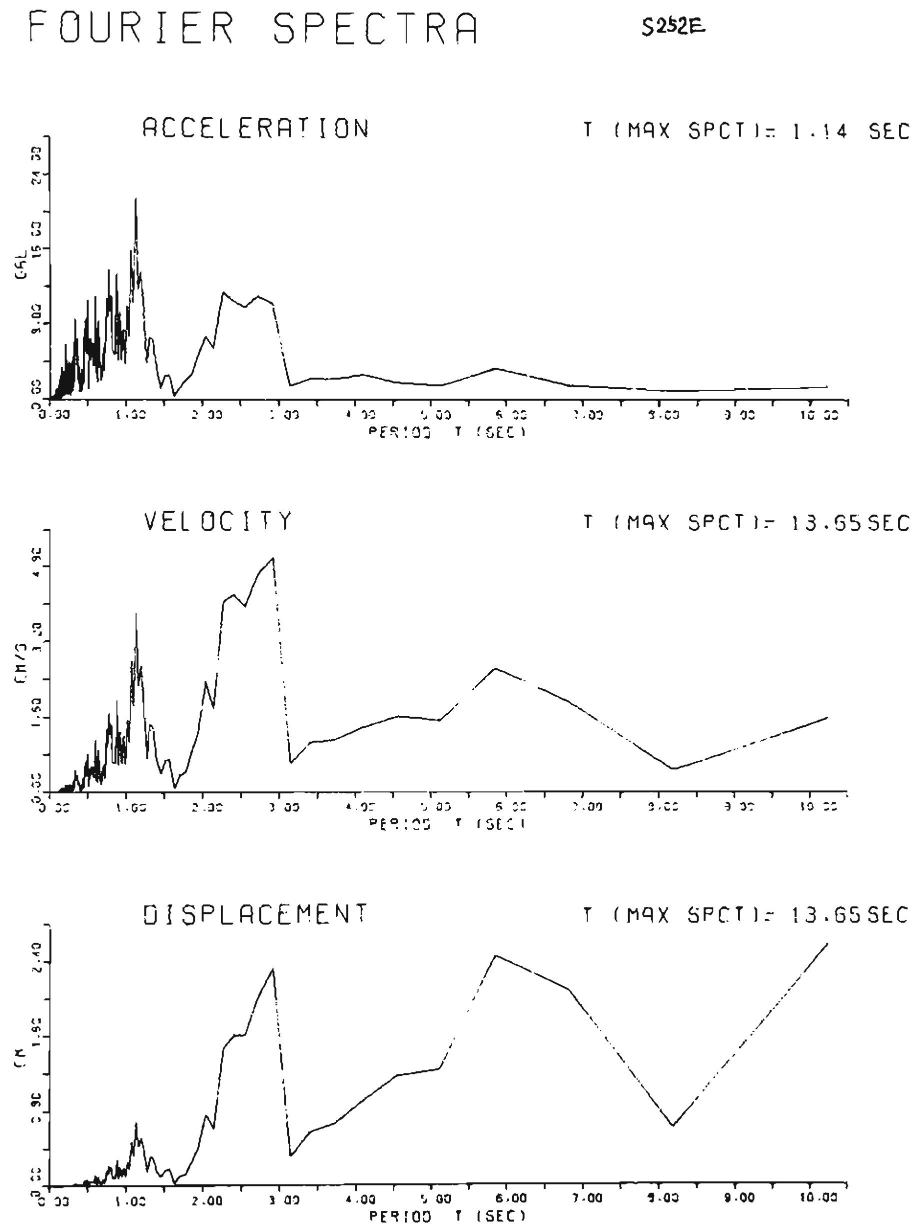
FOURIER SPECTRA
S252E
ACCELERATION
T (MAX SPCT)= 1.14 SEC
GAL
PERIOD T (SEC)
VELOCITY
T (MAX SPCT)= 13.65SEC
CM/S
PERIOD T (SEC)
DISPLACEMENT
T (MAX SPCT)= 13.65SEC
CM
PERIOD T (SEC)
0.00
1.00
2.00
3.00
4.00
5.00
6.00
7.00
8.00
9.00
10.00

Fig. A-27

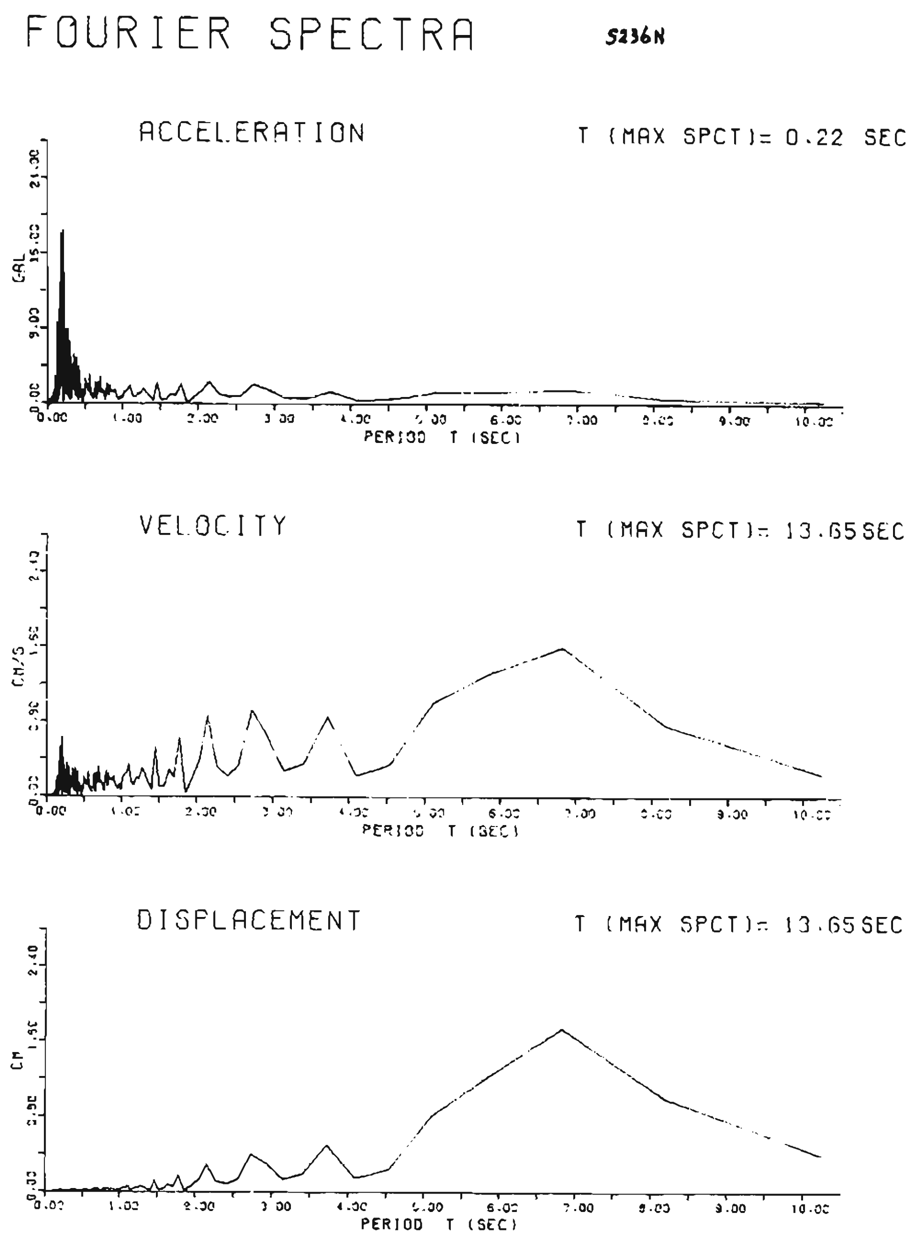
FOURIER SPECTRA
5236N
ACCELERATION
T (MAX SPCT)= 0.22 SEC
CAL
PERIOD T (SEC)
VELOCITY
T (MAX SPCT)= 13.65SEC
CM/S
PERIOD T (SEC)
DISPLACEMENT
T (MAX SPCT)= 13.65SEC
CM
PERIOD T (SEC)

Fig. A-28

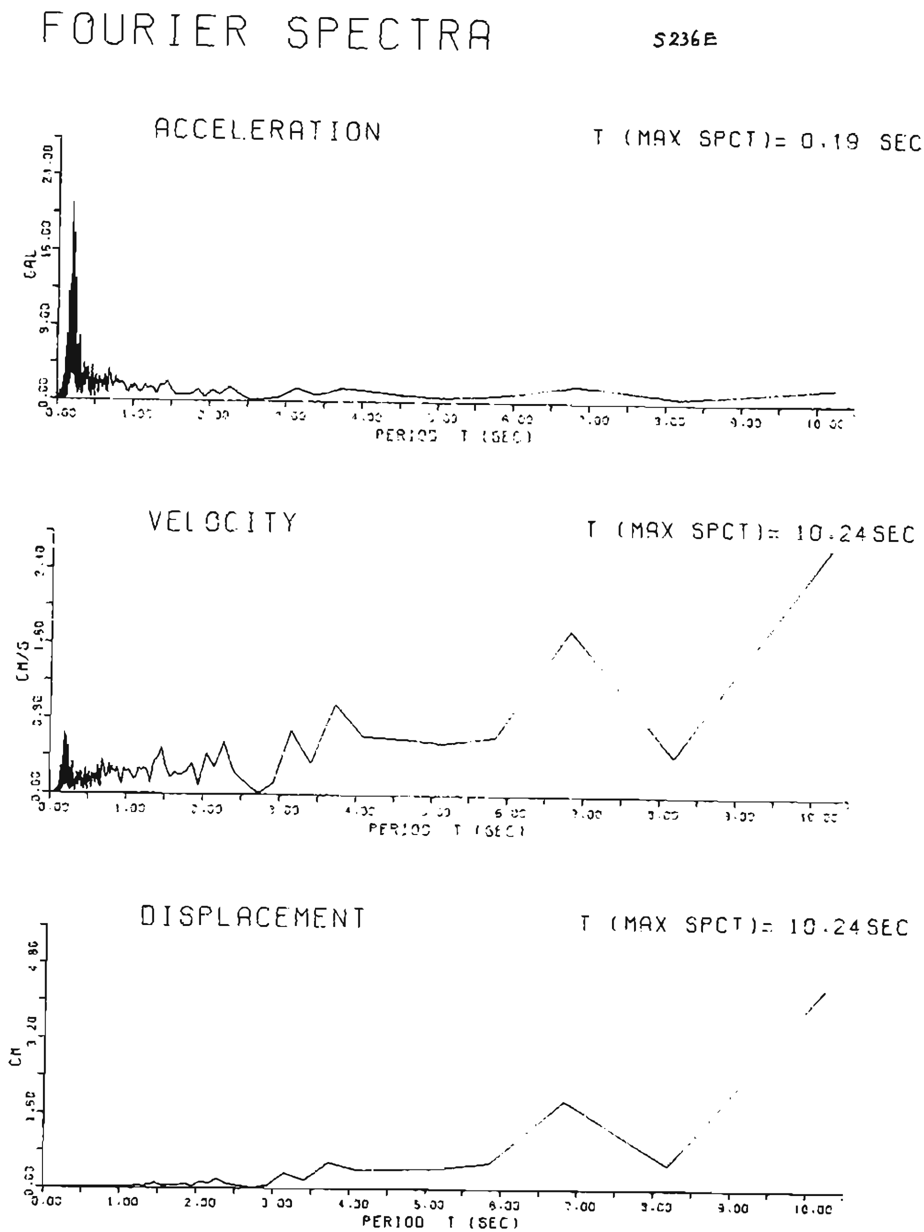
FOURIER SPECTRA
S236E
ACCELERATION
T (MAX SPCT)= 0.19 SEC
GAL
PERIOD T (SEC)
VELOCITY
T (MAX SPCT)= 10.24SEC
CM/S
DISPLACEMENT
T (MAX SPCT)= 10.24SEC
CM
0.00
1.00
2.00
3.00
4.00
5.00
6.00
7.00
8.00
9.00
10.00
PERIOD T (SEC)

Fig. A-29

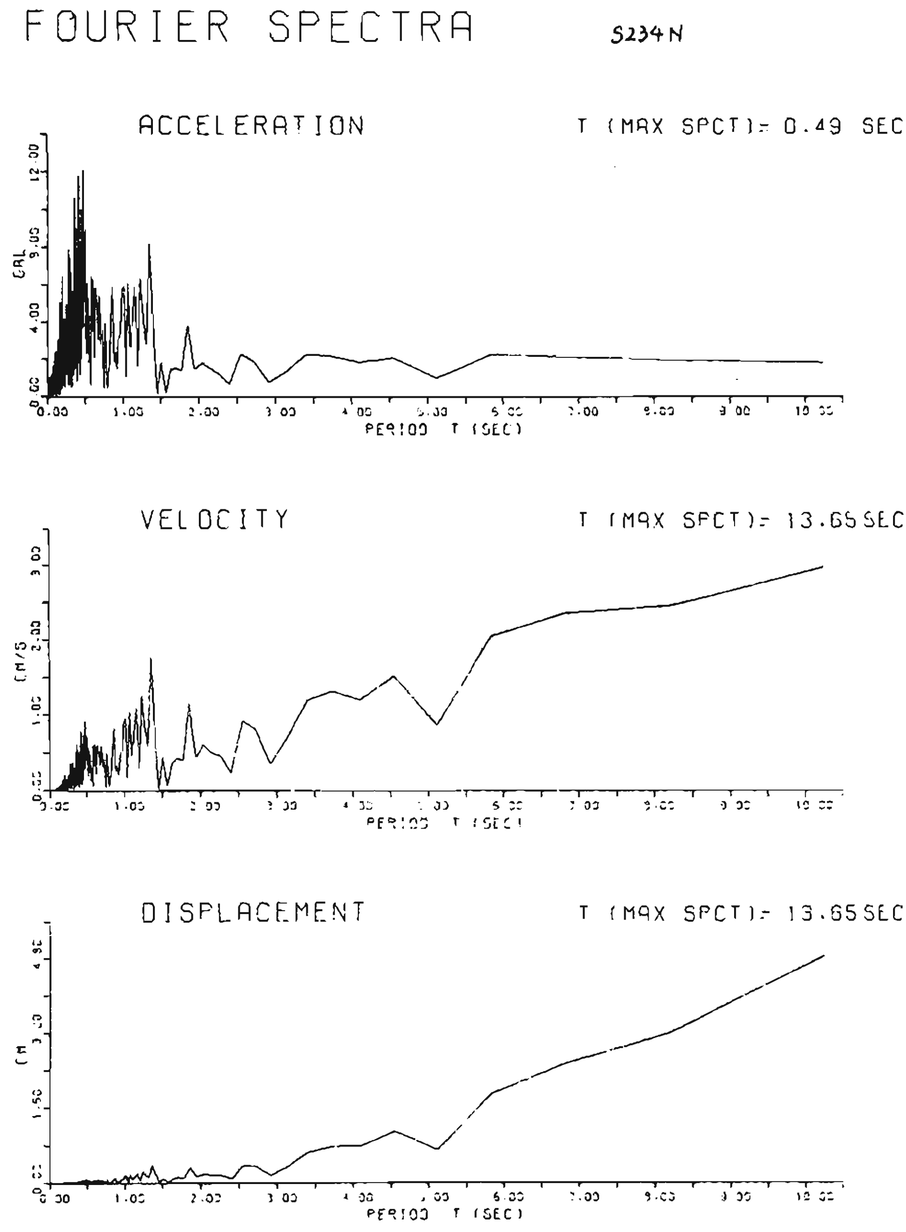
FOURIER SPECTRA
S234N
ACCELERATION
T (MAX SPCT)= 0.49 SEC
GAL
PERIOD T (SEC)
VELOCITY
T (MAX SPCT)= 13.65 SEC
CM/S
DISPLACEMENT
T (MAX SPCT)= 13.65 SEC
CM

Fig. A-30

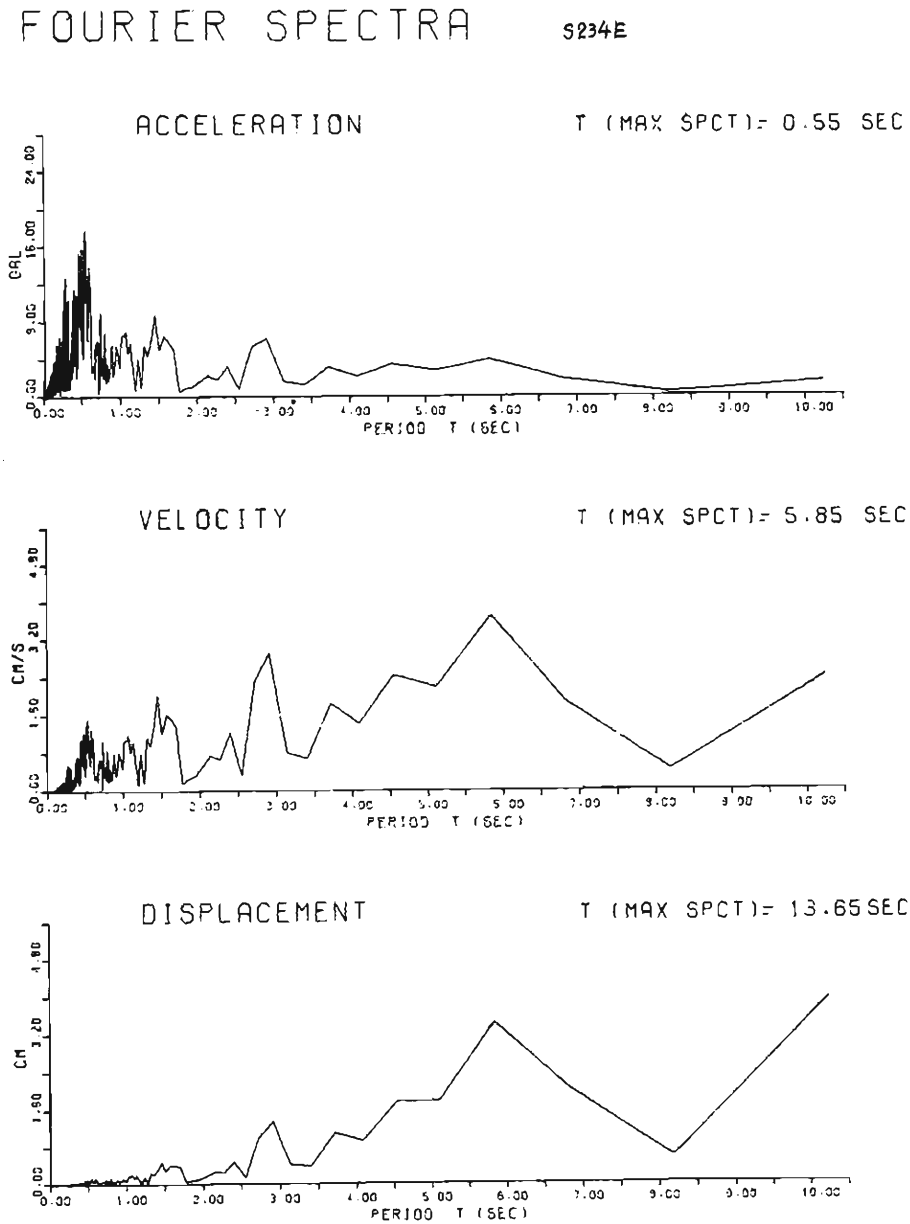
FOURIER SPECTRA
S234E
ACCELERATION
T (MAX SPCT)= 0.55 SEC
GAL
PERIOD T (SEC)
VELOCITY
T (MAX SPCT)= 5.85 SEC
CM/S
PERIOD T (SEC)
DISPLACEMENT
T (MAX SPCT)= 13.65 SEC
CM
PERIOD T (SEC)

Fig. A-31

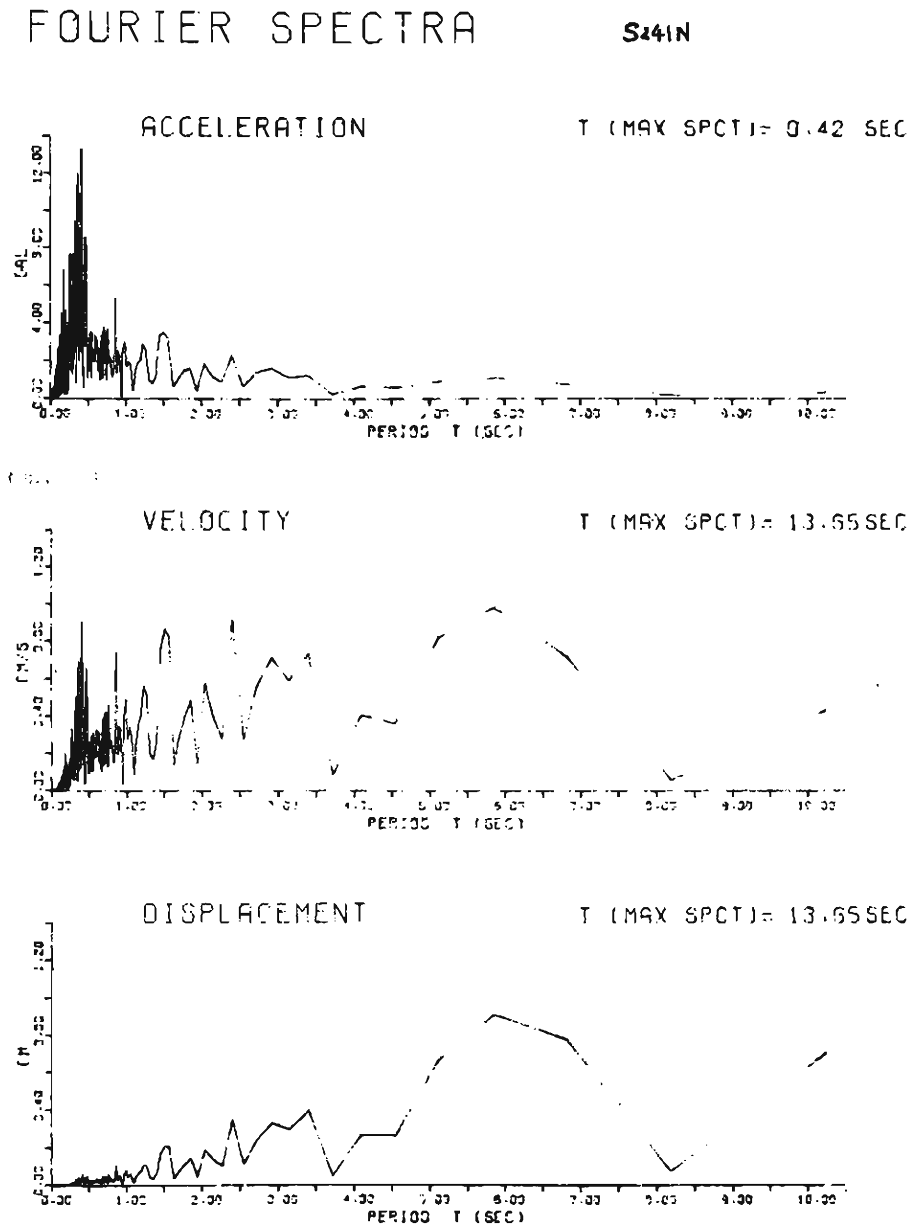
FOURIER SPECTRA
S241N
ACCELERATION
T (MAX SPCT)= 0.42 SEC
PERIOD T (SEC)
VELOCITY
T (MAX SPCT)= 13.65SEC
DISPLACEMENT
T (MAX SPCT)= 13.65SEC
PERIOD T (SEC)

Fig. A–32

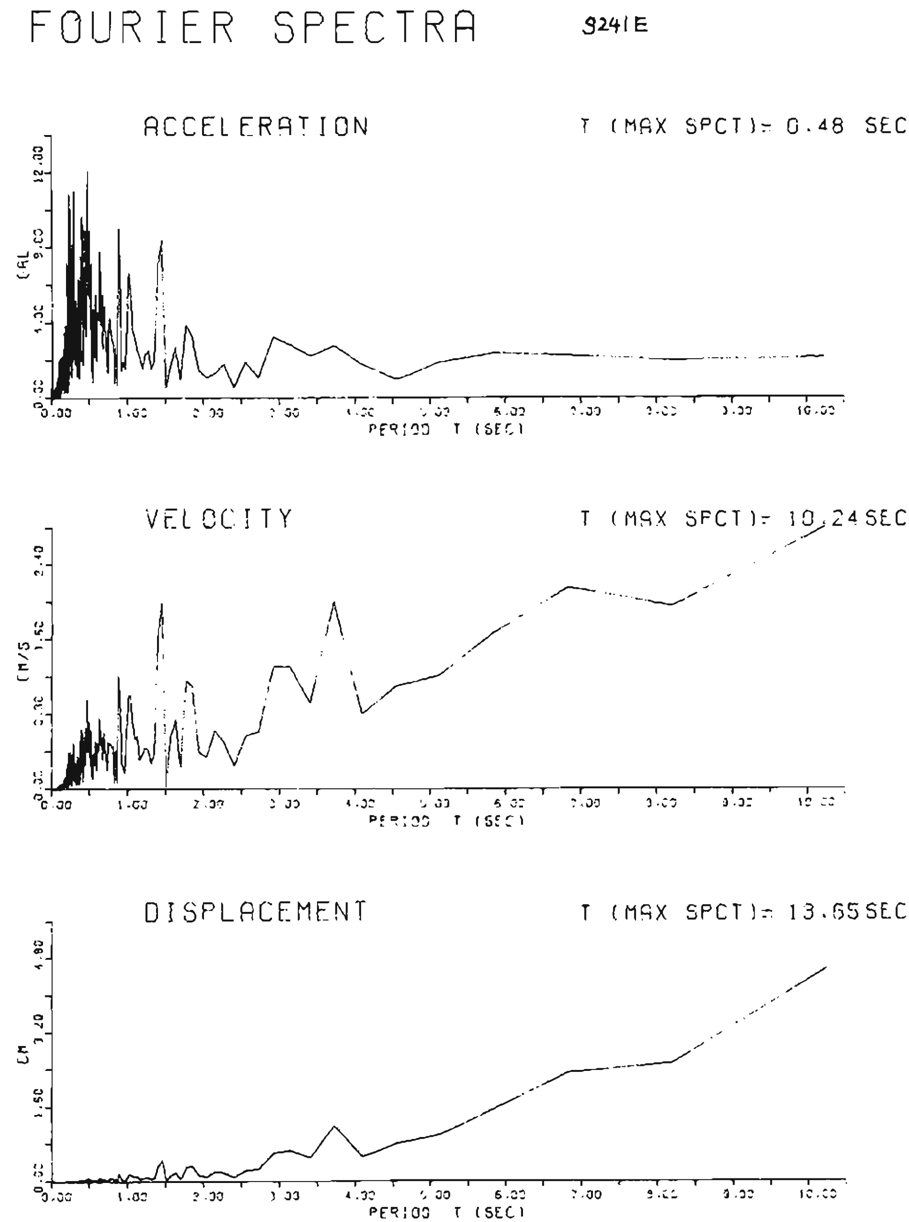
FOURIER SPECTRA
S241E
ACCELERATION
T (MAX SPCT)= 0.48 SEC
GAL
PERIOD T (SEC)
VELOCITY
T (MAX SPCT)= 10.24 SEC
CM/S
PERIOD T (SEC)
DISPLACEMENT
T (MAX SPCT)= 13.65 SEC
CM
PERIOD T (SEC)

Fig. A-33

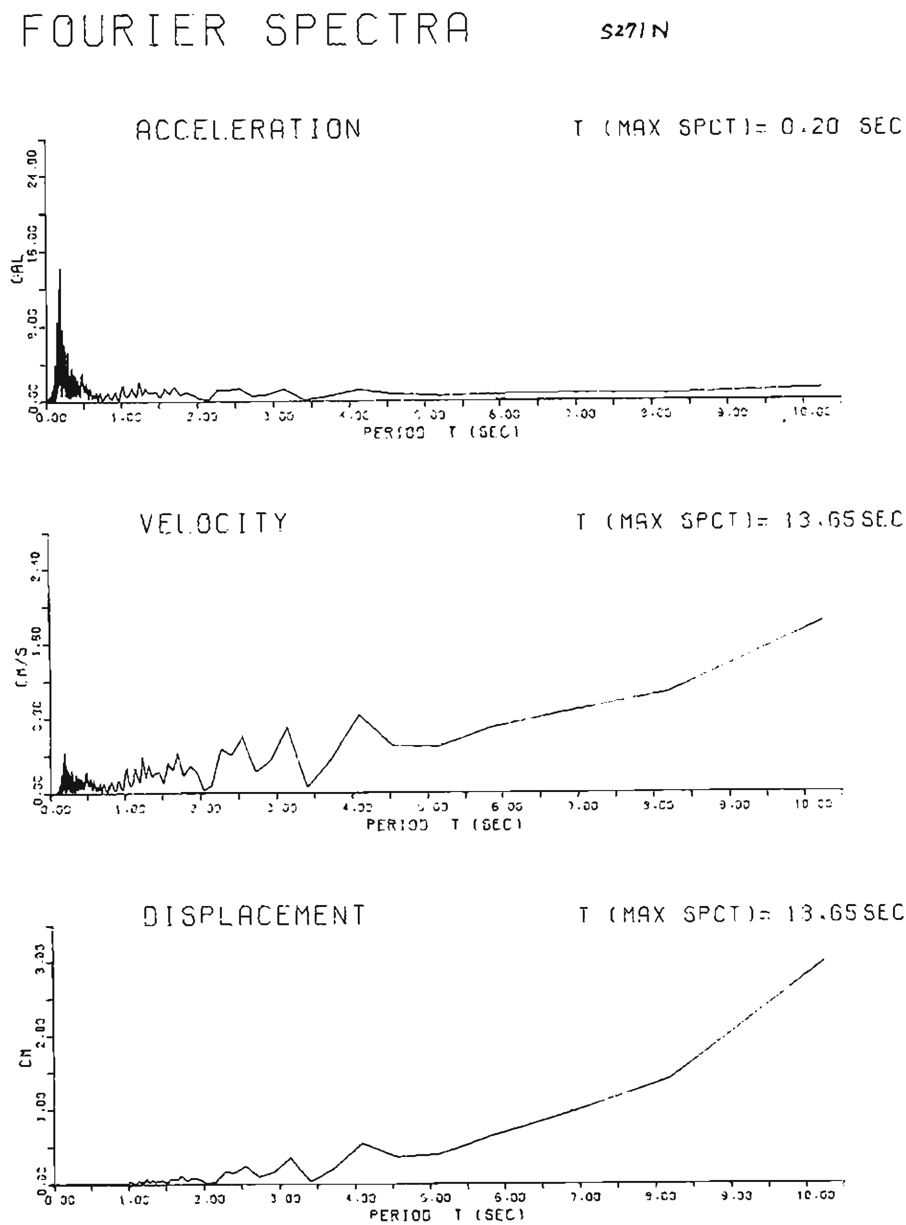
FOURIER SPECTRA
S271N
ACCELERATION
T (MAX SPCT)= 0.20 SEC
GAL
PERIOD T (SEC)
VELOCITY
T (MAX SPCT)= 13.65 SEC
CM/S
PERIOD T (SEC)
DISPLACEMENT
T (MAX SPCT)= 13.65 SEC
CM
PERIOD T (SEC)

Fig. A-34

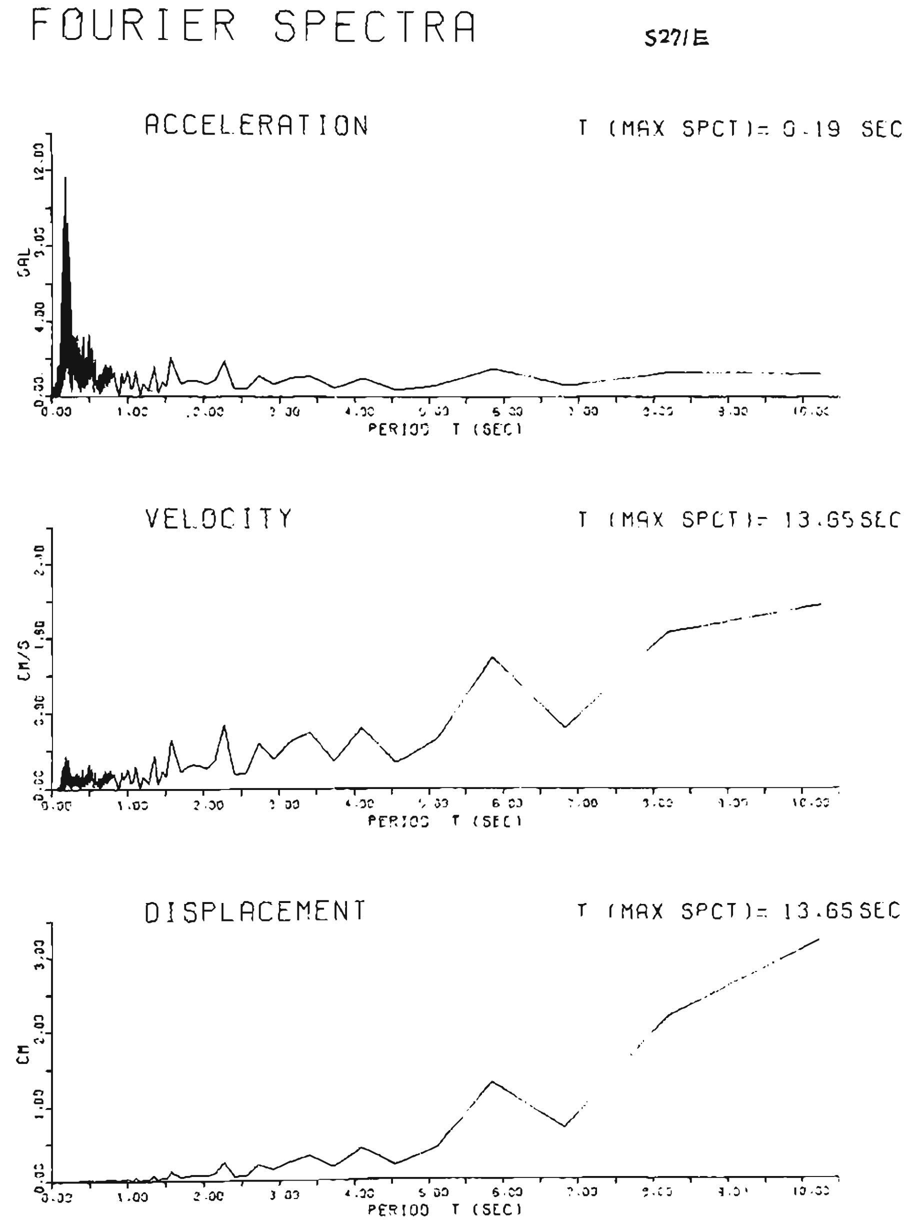
FOURIER SPECTRA
S27/E
ACCELERATION
T (MAX SPCT)= 0.19 SEC
SAL
PERIOD T (SEC)
VELOCITY
T (MAX SPCT)= 13.65 SEC
CM/S
PERIOD T (SEC)
DISPLACEMENT
T (MAX SPCT)= 13.65 SEC
CM
PERIOD T (SEC)

Fig. A-35

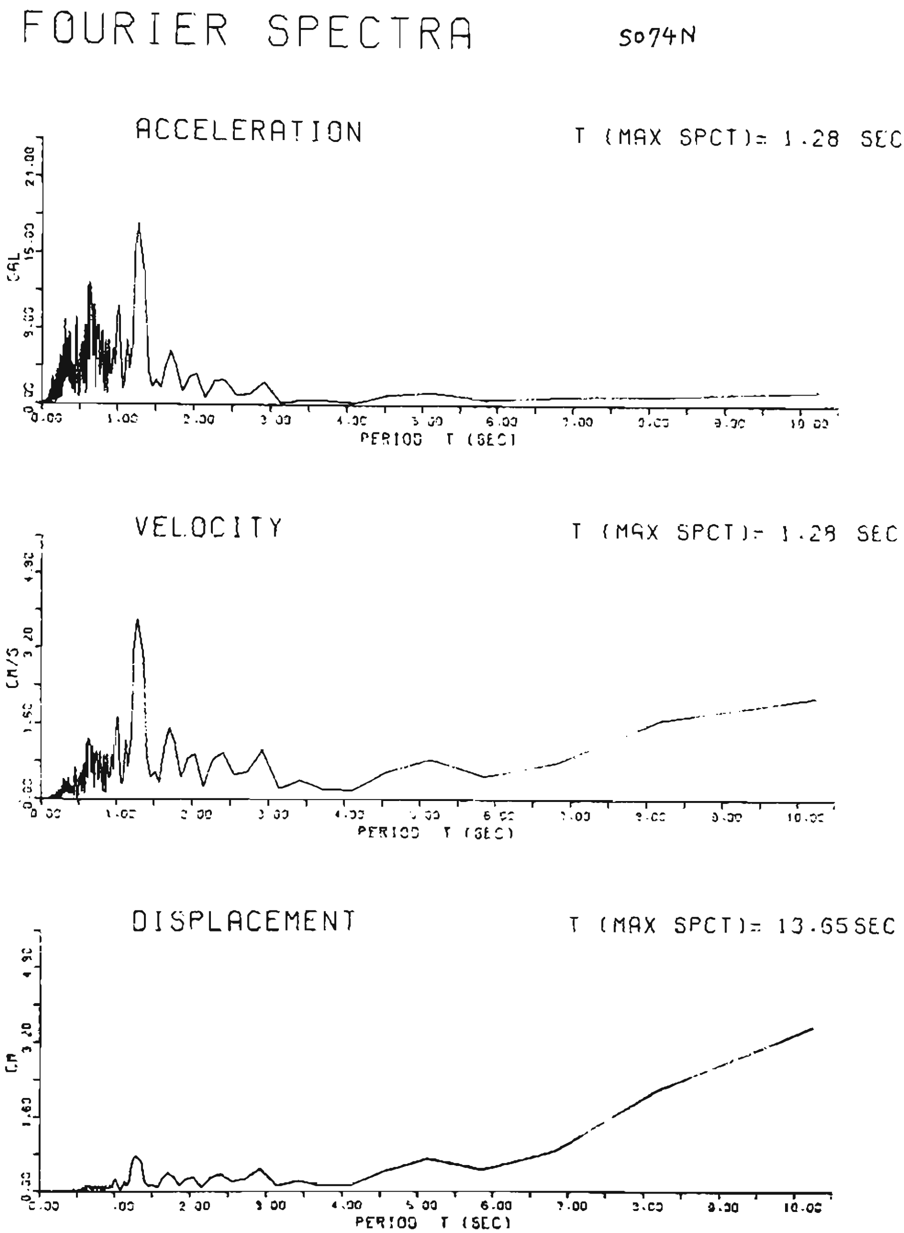
FOURIER SPECTRA
S074N
ACCELERATION
T (MAX SPCT)= 1.28 SEC
GAL
PERIOD T (SEC)
VELOCITY
T (MAX SPCT)= 1.28 SEC
CM/S
PERIOD T (SEC)
DISPLACEMENT
T (MAX SPCT)= 13.65SEC
CM
PERIOD T (SEC)

Fig. A-36

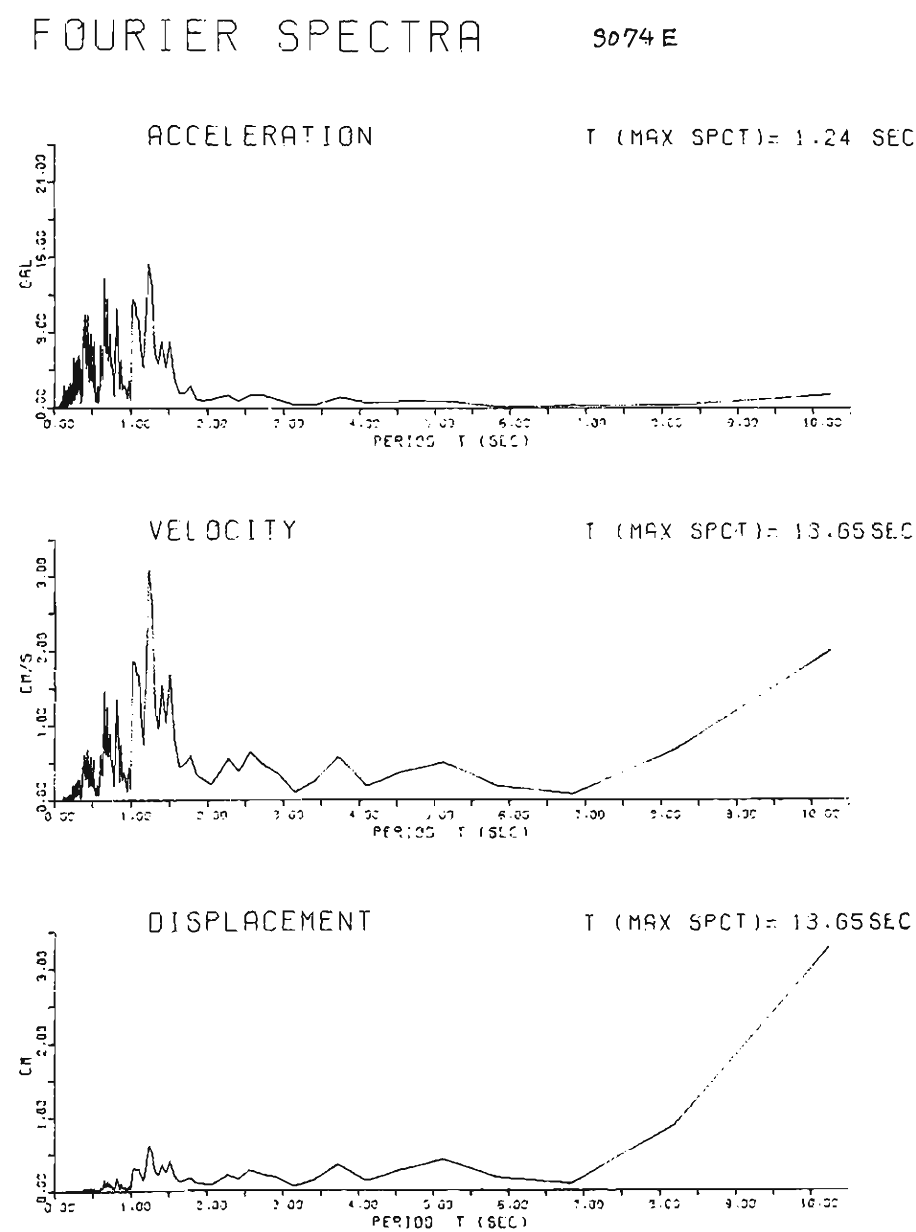
FOURIER SPECTRA
S074E
ACCELERATION
T (MAX SPCT)= 1.24 SEC
CAL
VELOCITY
T (MAX SPCT)= 13.65SEC
CM/S
DISPLACEMENT
T (MAX SPCT)= 13.65SEC
CM
PERIOD T (SEC)

Fig. A-37

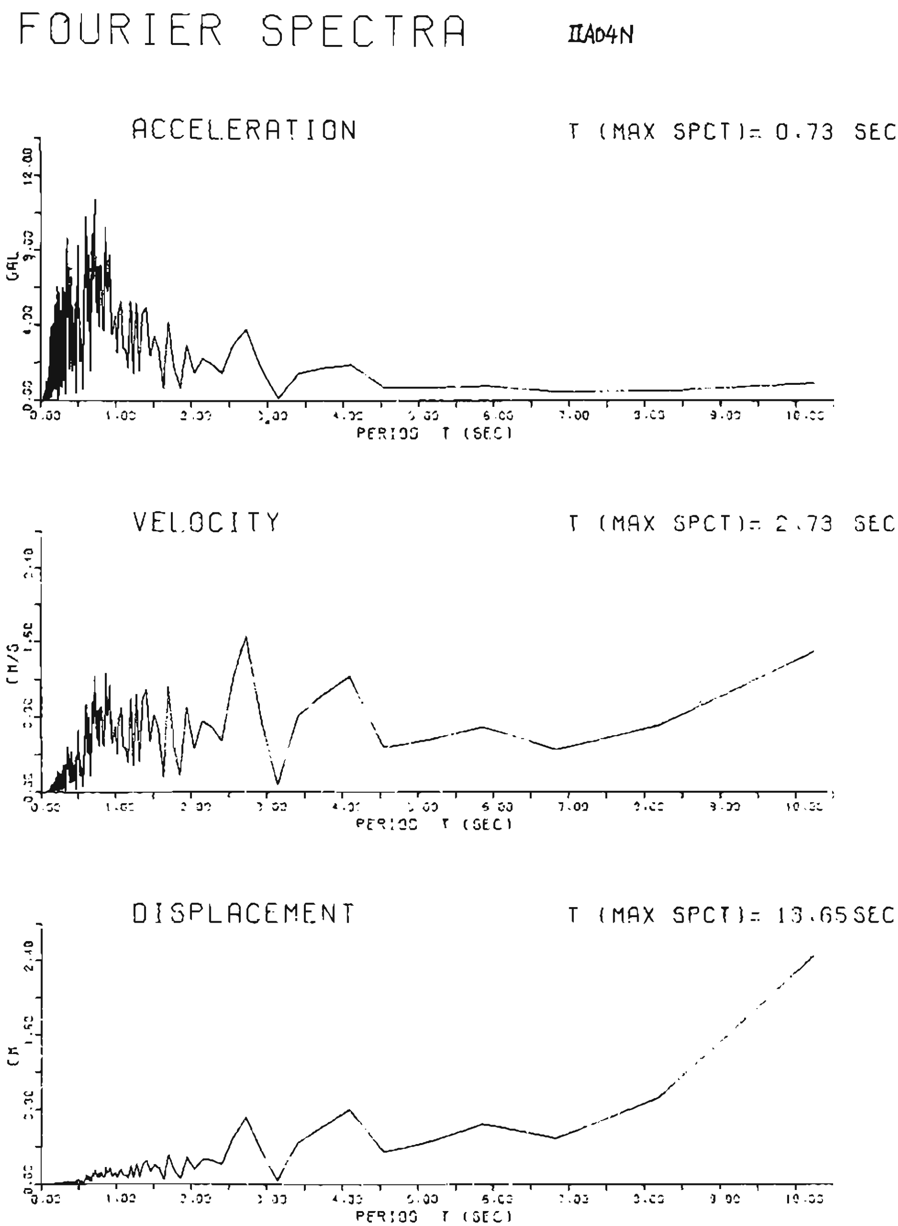
FOURIER SPECTRA
IIA04N
ACCELERATION
T (MAX SPCT)= 0.73 SEC
GAL
PERIOD T (SEC)
VELOCITY
T (MAX SPCT)= 2.73 SEC
CM/S
PERIOD T (SEC)
DISPLACEMENT
T (MAX SPCT)= 13.65SEC
CM
PERIOD T (SEC)

Fig. A-38